



**NAVAL  
POSTGRADUATE  
SCHOOL**

**MONTEREY, CALIFORNIA**

**THESIS**

**MICROSTRUCTURE SIGNATURE OF EQUILIBRIUM  
DOUBLE-DIFFUSIVE CONVECTION**

by

Shelley D Caplan

March 2008

Thesis Advisor:

Timour Radko

Second Reader:

Jeff Haferman

**Approved for public release; distribution is unlimited**

THIS PAGE INTENTIONALLY LEFT BLANK

**REPORT DOCUMENTATION PAGE**
*Form Approved OMB No. 0704-0188*

Public reporting burden for this collection of information is estimated to average 1 hour per response, including the time for reviewing instruction, searching existing data sources, gathering and maintaining the data needed, and completing and reviewing the collection of information. Send comments regarding this burden estimate or any other aspect of this collection of information, including suggestions for reducing this burden, to Washington Headquarters Services, Directorate for Information Operations and Reports, 1215 Jefferson Davis Highway, Suite 1204, Arlington, VA 22202-4302, and to the Office of Management and Budget, Paperwork Reduction Project (0704-0188) Washington DC 20503.

<b>1. AGENCY USE ONLY (Leave blank)</b>	<b>2. REPORT DATE</b> March 2008	<b>3. REPORT TYPE AND DATES COVERED</b> Master's Thesis
<b>4. TITLE AND SUBTITLE</b> Microstructure Signature of Equilibrium Double-Diffusive Convection		<b>5. FUNDING NUMBERS</b>
<b>6. AUTHOR(S)</b> Shelley D. Caplan		
<b>7. PERFORMING ORGANIZATION NAME(S) AND ADDRESS(ES)</b> Naval Postgraduate School Monterey, CA 93943-5000		<b>8. PERFORMING ORGANIZATION REPORT NUMBER</b>
<b>9. SPONSORING /MONITORING AGENCY NAME(S) AND ADDRESS(ES)</b> N/A		<b>10. SPONSORING/MONITORING AGENCY REPORT NUMBER</b>

**11. SUPPLEMENTARY NOTES** The views expressed in this thesis are those of the author and do not reflect the official policy or position of the Department of Defense or the U.S. Government.

<b>12a. DISTRIBUTION / AVAILABILITY STATEMENT</b> Approved for public release; distribution is unlimited	<b>12b. DISTRIBUTION CODE</b>
---	-------------------------------

**13. ABSTRACT (maximum 200 words)**

Salt fingering is an oceanographic small-scale phenomenon that occurs in statically stable regions where relatively warm salty water lies above cold, fresh water. Currently, analyses and interpretation of most microstructure measurements and salt fingers in particular, are based upon the fundamental assumption that the microstructure is isotropic. While it is generally accepted that the isotropic assumption may lead to underestimates of the dissipation rates of thermal and velocity fluctuations by factors of two to four, no significant attempt has been made to take the anisotropy of microstructure into account yet. Thus, the anisotropy remains one of the key elements of uncertainty in the microstructure analysis and a major obstacle in quantifying the strength of vertical mixing in the ocean.

This thesis represents an attempt to use direct numerical simulation in two and three-dimensions, in order to examine the validity of the isotropic assumption for the fully developed double-diffusive convection over a range of density ratios. Calculations are performed and the aspect ratio of the salt fingers is shown to be considerably different from unity. The anisotropy is particularly evident at higher density ratios. Based on the performed simulations, we formulate a simple method to take the anisotropy into account. The proposed technique is readily applicable to the oceanic data from free-falling and towed profilers. We expect that the reanalysis of microstructure with high density ratios would yield considerably different estimates of the diapycnal diffusivities and fluxes of heat and salt.

With regard to Navy interests, it should be noted that double diffusion can exert a substantial influence on the propagation and dispersion of the acoustic signature particularly in the regions of the pronounced thermocline staircases. Whether a sound source is transmitted from inside or outside a thermohaline staircase, the acoustic propagation is affected, especially at high frequencies.

<b>14. SUBJECT TERMS</b> double-diffusion, diffusive convection, flux		<b>15. NUMBER OF PAGES</b> 75	
<b>16. PRICE CODE</b>			
<b>17. SECURITY CLASSIFICATION OF REPORT</b> Unclassified	<b>18. SECURITY CLASSIFICATION OF THIS PAGE</b> Unclassified	<b>19. SECURITY CLASSIFICATION OF ABSTRACT</b> Unclassified	<b>20. LIMITATION OF ABSTRACT</b> UU

THIS PAGE INTENTIONALLY LEFT BLANK

**Approved for public release; distribution is unlimited**

**MICROSTRUCTURE SIGNATURE OF EQUILIBRIUM DOUBLE-DIFFUSIVE CONVECTION**

Shelley D. Caplan  
Lieutenant, United States Navy  
B.S., Old Dominion University, 1999

Submitted in partial fulfillment of the  
requirements for the degree of

**MASTER OF SCIENCE IN METEOROLOGY AND PHYSICAL  
OCEANOGRAPHY**

from the

**NAVAL POSTGRADUATE SCHOOL  
March 2008**

Author: Shelley Caplan

Approved by: Timour Radko  
Thesis Advisor

Jeff Haferman  
Second Reader

Mary L. Batteen  
Chairperson, Department of Oceanography

THIS PAGE INTENTIONALLY LEFT BLANK

## ABSTRACT

Salt fingering is an oceanographic small-scale phenomenon that occurs in statically stable regions where relatively warm salty water lies above cold, fresh water. Currently, analyses and interpretation of most microstructure measurements and salt fingers in particular, are based upon the fundamental assumption that the microstructure is isotropic. While it is generally accepted that the isotropic assumption may lead to underestimates of the dissipation rates of thermal and velocity fluctuations by factors of two to four, no significant attempt has been made to take the anisotropy of microstructure into account yet. Thus, the anisotropy remains one of the key elements of uncertainty in the microstructure analysis and a major obstacle in quantifying the strength of vertical mixing in the ocean.

This thesis represents an attempt to use direct numerical simulation in two and three-dimensions, in order to examine the validity of the isotropic assumption for the fully developed double-diffusive convection over a range of density ratios. Calculations are performed and the aspect ratio of the salt fingers is shown to be considerably different from unity. The anisotropy is particularly evident at higher density ratios. Based on the performed simulations, we formulate a simple method to take the anisotropy into account. The proposed technique is readily applicable to the oceanic data from free-falling and towed profilers. We expect that the reanalysis of microstructure with high density ratios would yield considerably different estimates of the diapycnal diffusivities and fluxes of heat and salt.

With regard to Navy interests, it should be noted that double diffusion can exert a substantial influence on the propagation and dispersion of the acoustic signature particularly in the regions of the pronounced thermocline staircases. Whether a sound source is transmitted from inside or outside a thermohaline staircase, the acoustic propagation is affected, especially at high frequencies.

THIS PAGE INTENTIONALLY LEFT BLANK

## TABLE OF CONTENTS

I.	INTRODUCTION.....	1
A.	DOUBLE DIFFUSION.....	1
B.	DYNAMICS OF SALT FINGERS.....	2
1.	Previous Research.....	4
2.	General Distribution of Double-diffusion.....	6
3.	Specific Examples.....	9
a.	<i>Mediterranean Outflow</i> .....	10
b.	<i>Brazil</i> .....	11
c.	<i>East China Sea</i> .....	12
C.	MEASURING MICROSTRUCTURE IN THE OCEAN. ....	13
D.	ISOTROPIC ASSUMPTION .....	14
E.	PROPOSED APPROACH .....	16
II.	THE MODEL DESCRIPTION .....	19
III.	DIRECT NUMERICAL SIMULATIONS IN TWO DIMENSIONS .....	23
A.	DEPENDENCE ON THE DENSITY RATIO.....	23
B.	DEPENDENCE ON THE LEWIS NUMBER.....	29
IV.	DIRECT NUMERICAL SIMULATIONS IN THREE DIMENSIONS .....	33
A.	MODEL DESCRIPTION.....	33
B.	DISTRIBUTION OF TEMPERATURE AND VERTICAL VELOCITY .....	33
C.	EQUILIBRATION OF THE SALT FINGER MAGNITUDE .....	36
V.	RESULTS .....	37
A.	TWO DIMENSIONS .....	37
1.	Heat and Salt Fluxes .....	37
2.	Vertical Anisotropy of Salinity and Temperature .....	40
3.	Anisotropy of Velocity .....	42
4.	Proposed Expressions for Temperature and Energy Dissipation .....	45
B.	THREE DIMENSIONS.....	46
1.	Anisotropy of Salinity and Temperature.....	46
C.	COMPARISON BETWEEN TWO AND THREE DIMENSIONAL SIMULATIONS .....	49
VI.	CONCLUSIONS .....	51
VII.	FUTURE STUDIES .....	53
	LIST OF REFERENCES .....	55
	INITIAL DISTRIBUTION LIST .....	59

THIS PAGE INTENTIONALLY LEFT BLANK

## LIST OF FIGURES

Figure 1.	Schematic diagram of salt finger development.....	2
Figure 2.	Numerical simulation of two-dimensional salt fingers. Light (dark) color is salty (fresh) water that is sinking (rising) ( <a href="http://www.planetwater.ca/research/oceanmixing/saltfingers.html">www.planetwater.ca/research/oceanmixing/saltfingers.html</a> ), Referenced March, 2008.....	3
Figure 3.	Theoretical wavelength $\lambda$ (Solid line) as function of $R_\rho$ for the fastest growing finger model (Kunze, 2003).....	5
Figure 4.	The schematic diagram illustrating dependence of Turner angle and density ratio on the vertical T-S gradients. From You (2002).....	6
Figure 5.	3D plot of (a) Tu: the color bar marks salt finger ( $45 < Tu < 90$ ), (b) diffusive convection and, (c) salt fingering only in the western (left-panel) and eastern (right-panel) Atlantic Ocean. Adopted from You (2002).....	7
Figure 6.	Same as Figure 5, but for Pacific Ocean.....	8
Figure 7.	Same as Figure 5, but for the Indian Ocean.....	9
Figure 8.	A region observed under the Mediterranean outflow where warm salty water overlies colder fresher water (from Turner, 1973).....	10
Figure 9.	Shadowgraph images of salt fingers each 5cm in diameter. Dark (light) bands are shadows of descending (rising) fingers, after (Williams, 1974).....	11
Figure 10.	BMC including red (blue) line that is warm (cold) South Atlantic Central Water (Antarctic Intermediate Water) .....	12
Figure 11.	CTD observations from high spatial resolution surveys. Thermohaline staircases indicated by a,b,c, and e . Shaded region $45 < Tu < 90$ correlates with $1 < R_\rho < 2$ and indicates salt finger regime. ....	12
Figure 12.	Vertical profiles of salinity (real line), temperature (dashed line), Turner angle (gray line) in the East China Sea at approximately 32N 129E (Shi and Wei, 2007).....	13
Figure 13.	The non-dimensional heat and salt fluxes (left panel), distribution of salt (upper right) and temperature perturbation (lower right) for $R_\rho = 1.1$ .....	24
Figure 14.	The same as in Fig.13 for $R_\rho = 1.3$ .....	25
Figure 15.	The same as in Fig.13 for $R_\rho = 1.5$ .....	26
Figure 16.	The same as in Fig.13 for $R_\rho = 1.7$ .....	27
Figure 17.	The same as in Fig.13 for $R_\rho = 1.9$ .....	28
Figure 18.	The same as in Fig.13 for $R_\rho = 2.1$ .....	29
Figure 19.	Same as Fig.13, however $\tau = 0.1$ and $R_\rho = 1.5$ .....	30
Figure 20.	The same as in Fig.15.....	31
Figure 21.	The same as in Fig.13, however $\tau = 0.01$ and $R_\rho = 1.5$ .....	32
Figure 22.	Temperature (top) and vertical velocity ('W' on bottom) in x-y (left) and x-z (right) planes, for $R_\rho = 1.1$ .....	34

Figure 23.	Same as Figure 22 above, for $R_\rho = 1.3$ .....	34
Figure 24.	Same as Figure 22 above, for $R_\rho = 1.5$ .....	35
Figure 25.	Same as Figure 22 above, for $R_\rho = 1.9$ .....	35
Figure 26.	Maximum departure of temperature from the mean (non-dimensional value). Coefficients $A_{TV}$ , $A_{TH}$ , $A_{VV}$ , $A_{VH}$ are calculated starting from the star, and on through equilibrium.....	36
Figure 27.	The non-dimensional heat and salt fluxes as a function of density ratio for $\tau = 0.1$ . Note that both heat and salt fluxes decrease with $R_\rho$ .....	38
Figure 28.	The same as in Fig. 27 but for $\tau = 0.03$ .....	38
Figure 29.	The same as in Fig. 27 but for $\tau = 0.01$ .....	39
Figure 30.	The non-dimensional heat and salt fluxes as a function of $\tau$ for $R_\rho = 1.5$ . Note the increase in fluxes with decreasing $\tau$ .....	39
Figure 31.	The vertical anisotropy coefficients for temperature ( $A_{TV}$ ) and salinity ( $A_{SV}$ ) as a function of the density ratio ( $R_\rho$ ) for $\tau = 0.1$ .....	40
Figure 32.	The same as in Fig. 31 but for $\tau = 0.03$ .....	41
Figure 33.	The same as in Fig. 31 but for $\tau = 0.01$ .....	41
Figure 34.	Vertical Anisotropy coefficients as a function of $\tau$ for $R_\rho = 1.5$ .....	42
Figure 35.	The anisotropy of velocity coefficients for vertical ( $A_{VV}$ ) and horizontal ( $A_{VH}$ ) directions, as a function of the density ratio ( $R_\rho$ ) for $\tau = 0.1$ .....	43
Figure 36.	The same as in Fig. 35 but for $\tau = 0.03$ .....	43
Figure 37.	The same as in Fig. 35 but for $\tau = 0.01$ .....	44
Figure 38.	Anisotropy of velocity coefficients as a function of $\tau$ for $R_\rho = 1.5$ .....	44
Figure 39.	The 3D vertical anisotropy coefficients for temperature ( $A_{TV}$ ) and salinity ( $A_{SV}$ ) as a function of the density ratio ( $R_\rho$ ) for $\tau = 0.03$ .....	46
Figure 40.	The horizontal anisotropy coefficients for temperature ( $A_{TH}$ ) and salinity ( $A_{SH}$ ) as a function of the density ratio ( $R_\rho$ ) for $\tau = 0.03$ .....	47
Figure 41.	The anisotropy of velocity coefficients for vertical ( $A_{VV}$ ) and horizontal ( $A_{VH}$ ) directions as a function of density ratio for $\tau = 0.03$ .....	48

## LIST OF TABLES

Table 1.	Proposed 2D anisotropic coefficients as a function of $R_\rho$ for $\tau = 0.01$ .....	45
Table 2.	Proposed 3D anisotropic coefficients as a function of $R_\rho$ for $\tau = 0.03$ .....	48

THIS PAGE INTENTIONALLY LEFT BLANK

## **ACKNOWLEDGMENTS**

It was both a challenging and rewarding experience to learn how to use numerical modeling in order to study double diffusion. I would like to take the opportunity to express a very sincere thank you to those whom made this experiment possible.

After taking Fluid Dynamics with Dr. Timour Radko and watching his technique, style, and ease of communicating very complicated subject matter, I became very interested in studying my thesis under his supervision. With Dr. Radko's subject expertise in field of salt fingers, he was able to provide superb guidance, theoretical explanations, and assistance as needed.

Whenever I had trouble with the high performance computing resources, Dr. Jeffrey Haferman skillfully and patiently taught me how to solve those problems, and gave me the tools to better solve them in the future.

Lastly, I would like to thank friends and family who supported me throughout this entire process and have patiently stood by my side.

THIS PAGE INTENTIONALLY LEFT BLANK

## I. INTRODUCTION

### A. DOUBLE DIFFUSION

Double diffusive convection is a term commonly used to describe a set of phenomena caused by the presence of two different density components with different molecular diffusivities. Double diffusive convection was first discovered in the oceanographic context, where the two differing components are temperature and salinity. It has since been recognized to have scientific applications in other areas such as geology, astrophysics, and fluid dynamics. For example, in the geological context, double diffusion occurs at the boundary between the Earth's mantle and the core.

There are two forms of oceanic double diffusion, salt fingering and diffusive convection. Salt fingering occurs when both temperature and salinity increase upward. The reverse of the salt finger case is diffusive convection, where cold fresh water overlies warm salty water. Diffusive convection is more common in high-latitude regions such as the Beaufort Gyre of Arctic Ocean. However, this thesis is focused more on the salt finger regime of double diffusive convection.

The significance of the effects of two diffusing density components was first recognized by Stommel et al. (1956), which was followed by the rigorous analysis of the resulting instabilities by Stern (1960). Double diffusive convection in the ocean leads to transport of water properties such as heat and salt. The consequences of the double diffusive oceanic mixing for a global scale circulation are still unknown and highly controversial. However, it is often assumed, in the ocean, double diffusive convection is significant for maintainance of the thermocline and affects the meridional overturning circulation. Thermohaline staircases, the well defined steps in vertical temperature and salinity profiles, are also commonly attributed to double diffusion.

With regard to Navy interests, it should be noted that double diffusion can exert a substantial influence on the propagation and dispersion of the acoustic signature particularly in the regions of the pronounced thermocline staircases (Wall, 2007). Whether a sound source is transmitted from inside or outside a thermohaline staircase, the acoustic propagation is affected, especially at high frequencies.

## B. DYNAMICS OF SALT FINGERS

In warm climates such as the tropics and/or subtropics, evaporation accompanied by solar heating at the sea surface, causes a layer of relatively warm, salty water to develop. Deeper beneath this layer, there may reside a cooler, fresher layer of water which was transported from the poles by thermohaline circulation. Thus in this case, heat is the stabilizing and salt is considered the destabilizing component. The stratified interface between these two layers is statically stable. However, because heat has a molecular diffusion rate ( $1.4 \times 10^{-7} \text{ m}^2 \text{s}^{-1}$ ) 100 times faster than the molecular diffusivity of salt ( $1.1 \times 10^{-9} \text{ m}^2 \text{s}^{-1}$ ), the flow develops a new type of instability, which is described as follows.

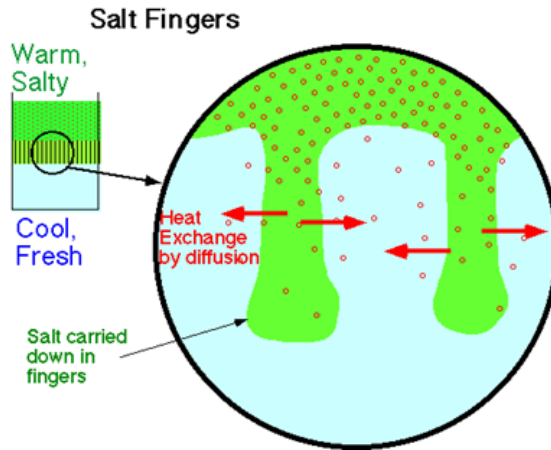


Figure 1. Schematic diagram of salt finger development

When a parcel of water is removed from equilibrium, it is affected by the diffusion of heat and salt across its boundary (see Fig. 1). The parcel rapidly loses its heat but retains the slowly diffusing salt. Consequently, the parcel displaced downward becomes denser and sinks farther into the lower layer while a parcel from the less dense lower layer rises into voids left by the parcel. Thus, instead of the parcel returning upward to equilibrium, it continues its motion downward due to its increased density, and this motion is what forms a salt finger. Stern (1960) first systematically analyzed these instabilities and described how the sinking and rising motions occur in narrow vertical columns that have become known as salt fingers.

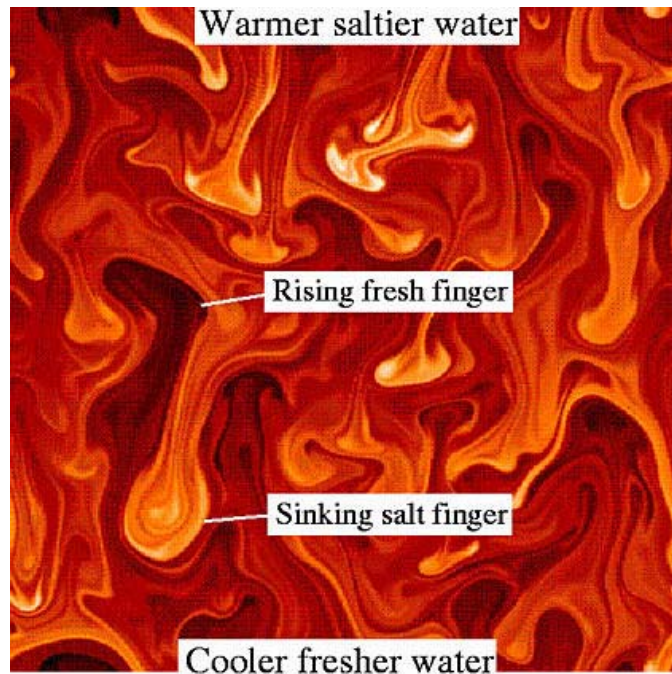


Figure 2. Numerical simulation of two-dimensional salt fingers. Light (dark) color is salty (fresh) water that is sinking (rising) ([www.planetwater.ca/research/oceanmixing/saltfingers.html](http://www.planetwater.ca/research/oceanmixing/saltfingers.html)), Referenced March, 2008.

## 1. Previous Research

Salt fingers have been extensively studied theoretically and experimentally. Stommel et al. (1956) first formulated a concept of a salt fountain. In this paper, the authors described how a perpetual salt fountain would ensue after inserting a long pipe deep into the ocean that could upwell deep cold fresh water with no external energy source to the ocean surface. A few years later, Stern (1960) proposed that double-diffusive convection could be maintained in the absence of Stommel's pipe, and supported his conclusion by linear stability analysis. Later on, salt fingers were produced in the lab experimentally by Turner and Stommel (1964). The first two dimensional salt fingers were created with direct numerical simulation (DNS) by Piacsek and Toomre (1980). Studies in three dimensions have been continued by Radko and Stern (1999), Yoshida and Nagashima (2003), and others referenced therein.

Stern (1960) and Turner (1965) suggested that the existence and intensity of double diffusion and salt fingering is controlled by the so-called density ratio  $R_\rho$ , defined as:

$$R_\rho = \frac{\alpha T_z}{\beta S_z} \quad (1)$$

where  $\alpha = -\frac{1}{\rho} \left( \frac{\partial \rho}{\partial T^*} \right)_{S^*, P^*}$  is the coefficient of thermal expansion, and  $\beta = \frac{1}{\rho} \left( \frac{\partial \rho}{\partial S^*} \right)_{T^*, P^*}$  is the coefficient of saline contraction, and  $S_z$  and  $T_z$  are the vertical temperature and salinity gradients, respectively. Theoreticians, numerical modelers, and experimentalists have reached the agreement that density ratio is the single most important parameter controlling all aspects of salt fingers. Density ratio is defined as the temperature/salinity gradient normalized by the expansion/contraction coefficients. As  $R_\rho$  increases, fluxes decrease, and salt fingers are strongest when  $R_\rho \sim 1$ .

Kunze (2003) summarized his findings and those of others and found that flux ratios, wavelengths ( $\lambda$ ), and even growth rates observed in most laboratory experiments and numerical simulations are consistent with those of the fastest-growing fingers. The fastest-growing finger model, for instance, explicitly predicts the unique dependencies of the flux ratios and growth rates on the density ratios, as indicated in Figure 3. Numerical simulations find tall well-ordered salt fingers exist at higher density ratios, which become shorter and more disorganized as  $R_\rho$  approaches one. The strong dependence of the salt finger patterns on the density ratio will be profitably explored in our study as well.

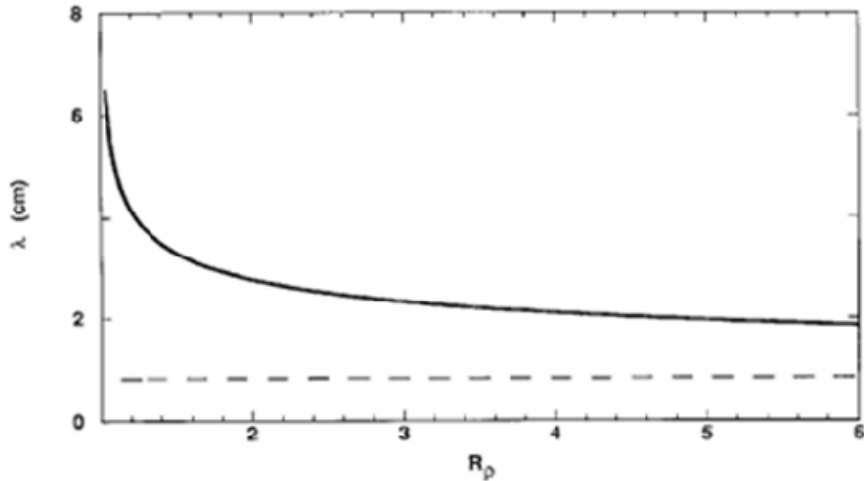


Figure 3. Theoretical wavelength  $\lambda$  (Solid line) as function of  $R_\rho$  for the fastest growing finger model (Kunze, 2003).

For some applications, it is more convenient to use, instead of density ratio, a related quantity  $Tu$ , known as the Turner angle (Ruddick, 1983).

$$Tu(\text{deg}) = \tan^{-1} \left( \alpha \frac{\partial T}{\partial z} - \beta \frac{\partial S}{\partial z}, \alpha \frac{\partial T}{\partial z} + \beta \frac{\partial S}{\partial z} \right). \quad (2)$$

$R_\rho$  can be expressed in terms of the Turner angle as follows:

$$R_\rho = -\tan(Tu + 45). \quad (3)$$

The Turner angle is shown in Figure 3, and the range  $45^\circ < Tu < 90^\circ$  ( $1 < R_p < 100$ ) represents the regime which favors the spontaneous formation of salt fingers.

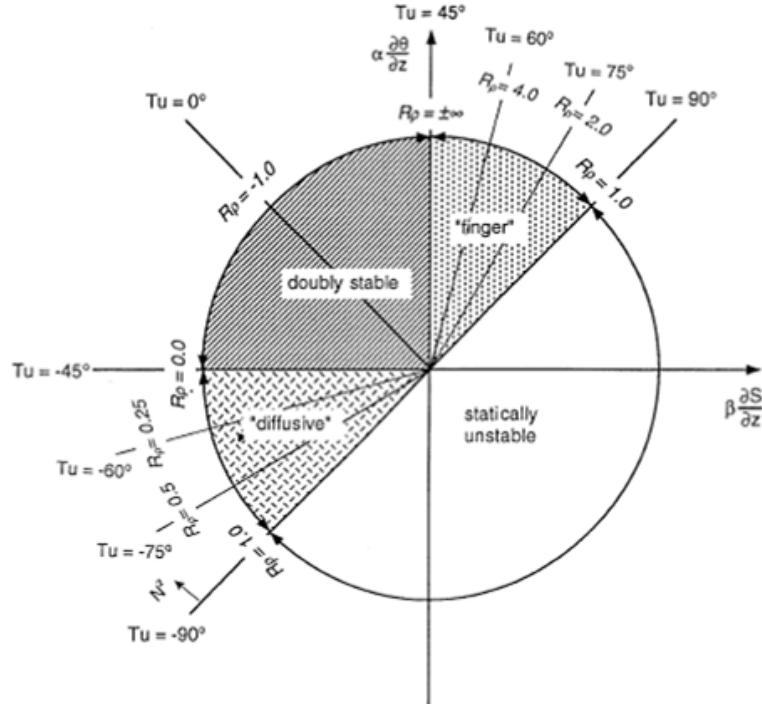


Figure 4. The schematic diagram illustrating dependence of Turner angle and density ratio on the vertical T-S gradients. From You (2002).

## 2. General Distribution of Double-diffusion

In Figure 5, You (2002) uses Turner angle to describe regions susceptible for double diffusion. Turner calculated  $Tu$  for three oceans from the 1994 Levitus climate atlas. 50% of the world's oceans contain double diffusion, and two thirds of that is salt fingers (Kluikov and Karlin, 1995). Additionally, estimates indicate that 90% of the Atlantic thermocline is favorable for salt finger formation.

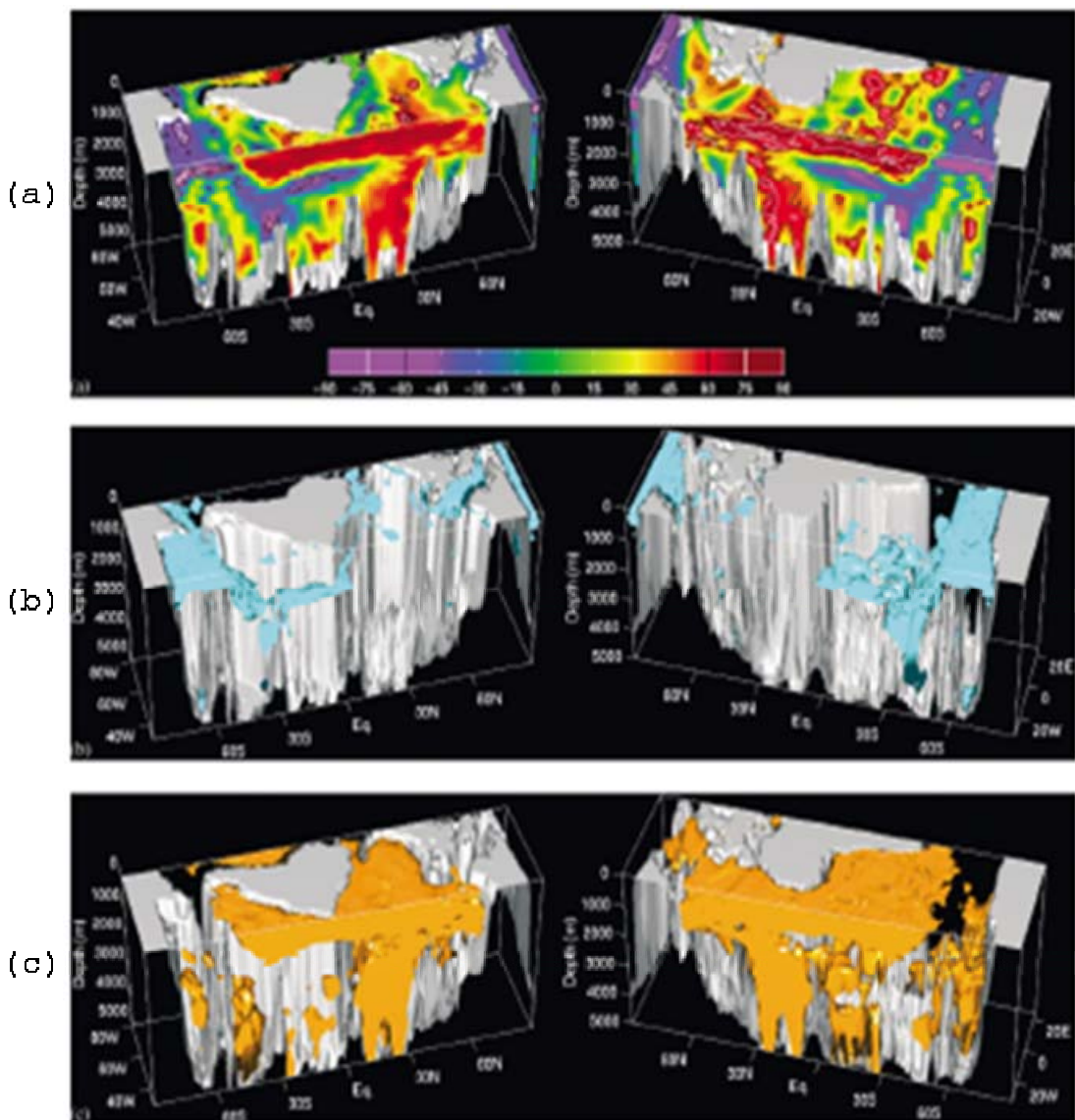


Figure 5. 3D plot of (a) Tu: the color bar marks salt finger ( $45 < Tu < 90$ ), (b) diffusive convection and, (c) salt fingering only in the western (left-panel) and eastern (right-panel) Atlantic Ocean. Adopted from You (2002).

Figure 6 indicates regions in the Pacific Ocean known for double diffusion.

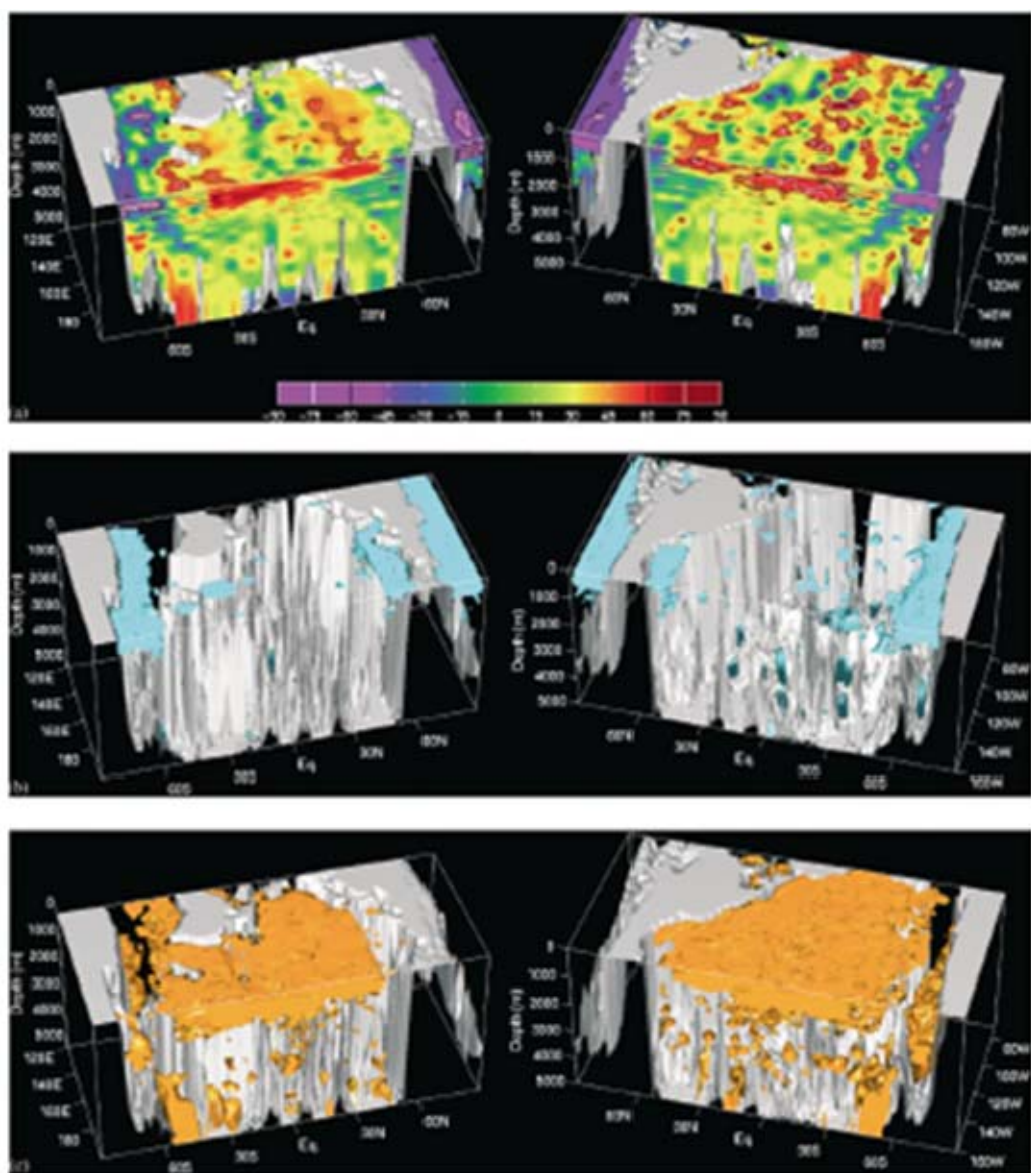


Figure 6. Same as Figure 5, but for Pacific Ocean

Figure 7 indicates regions in the Indian Ocean known for double diffusion.

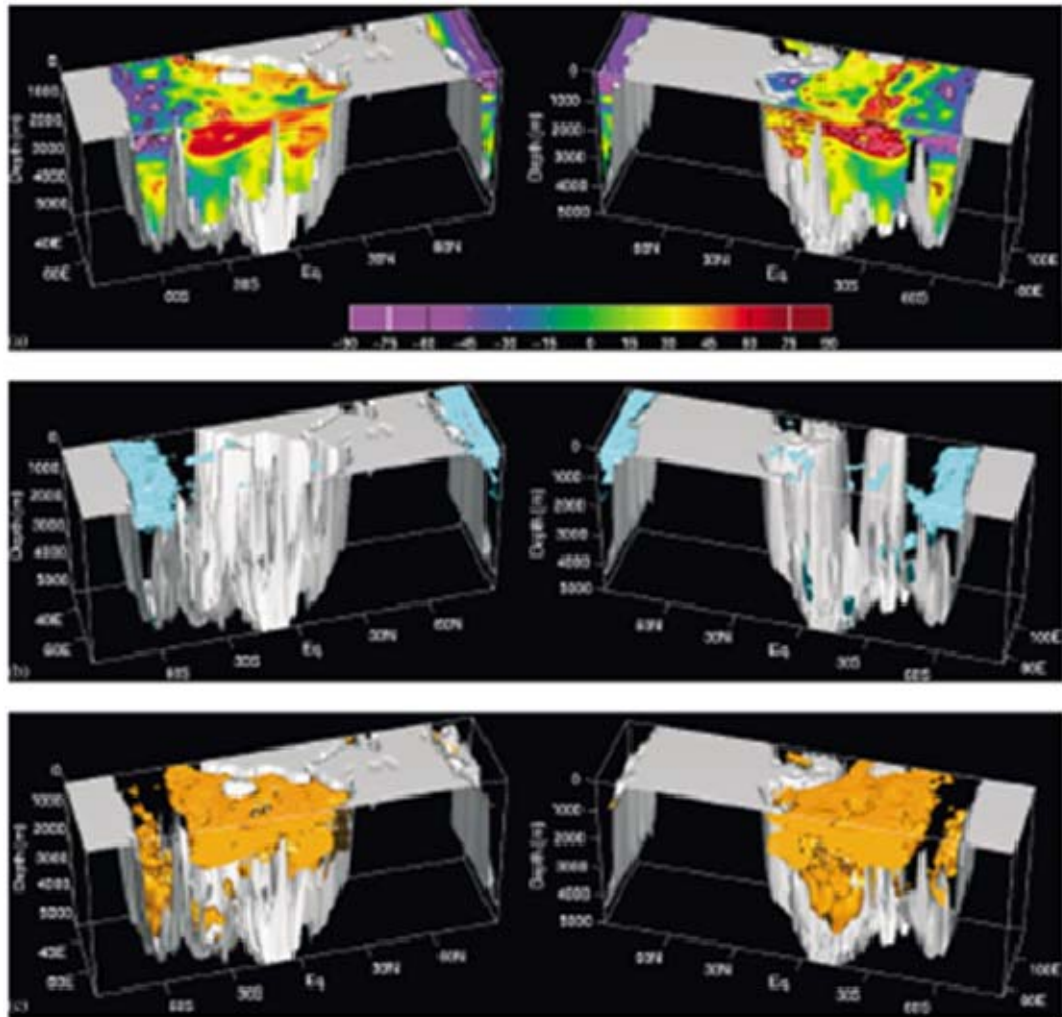


Figure 7. Same as Figure 5, but for the Indian Ocean.

### 3. Specific Examples

With technological advancements over the past few decades, oceanographers around the world have been observing salt fingers using different techniques. Some have used continuously recording temperature-salinity-depth devices. Others have used tracers released such as sulfur hexafluoride ( $SF_6$ ) to monitor diapycnal mixing (Schmitt et. al., 2005). Salt fingers have been identified in regions throughout the world.

### a. Mediterranean Outflow

Due to the fact that in the Mediterranean, evaporation exceeds precipitation, a warm and salty body of water exists. The Mediterranean Sea is in fact, warmer and saltier than most other bodies of water. When this Mediterranean water flows out into the Atlantic Ocean through the Straights of Gibraltar, it creates a salinity maximum below the sea surface. It is in this region of the Eastern Atlantic the water is stratified such that there is warm salty (Mediterranean) water overlying cold fresh (Atlantic Intermediate) water. This is one of the most studied cases of salt fingering in the ocean.

Tait and Howe (1968, 1971) first recorded salt fingers in the Atlantic Ocean deep below the Mediterranean outflow, where warm salty layer overlies a colder fresher layer. They noticed existence of the pronounced thermohaline staircases with the typical step height of 20m – a signature of the particularly active double-diffusive convection (Fig. 8).

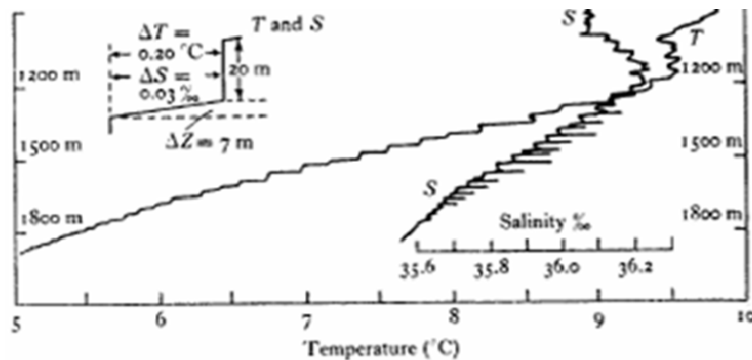


Figure 8. A region observed under the Mediterranean outflow where warm salty water overlies colder fresher water (from Turner, 1973).

Soon after, Williams (1974) optically observed salt fingers underneath the Mediterranean outflow. In a region below the salinity maximum, where temperature and salinity both decreased with depth, he was able to photograph narrow elongated structures 6mm in diameter and 24cm in length, which he interpreted as fully developed salt fingers. In Figure 9, shadowgraph images of salt fingers are shown.

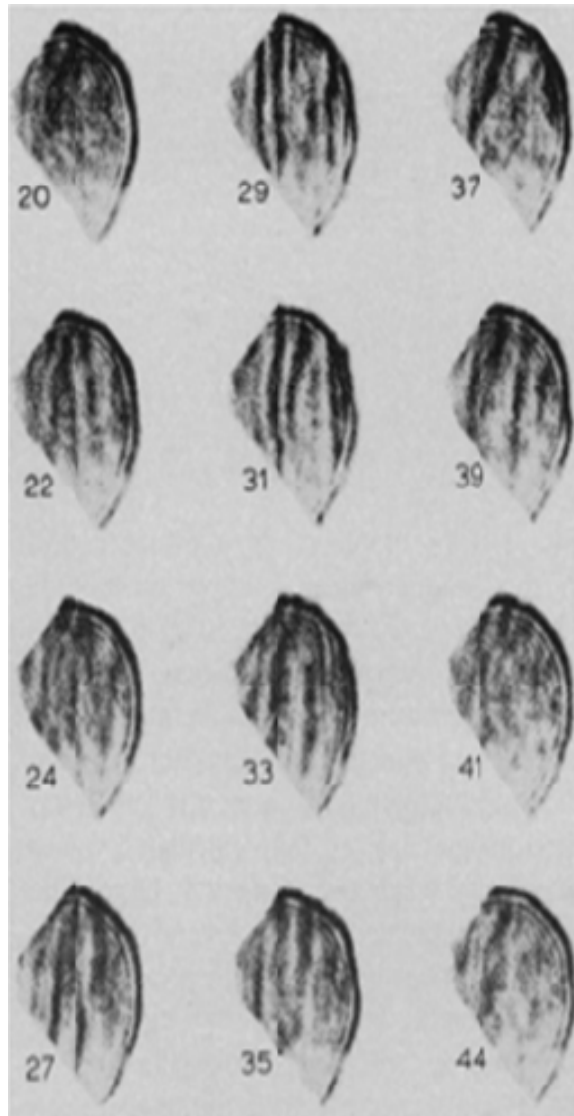


Figure 9. Shadowgraph images of salt fingers each 5cm in diameter. Dark (light) bands are shadows of descending (rising) fingers, after (Williams, 1974).

**b. Brazil**

The presence of salt fingers has been suggested by Bianchi et al. (2002) in the Brazil-Malvinas Confluence (BMC) based on observations of thermohaline staircases and low density ratios. There exists warm salty South Atlantic Central Water over cold fresh Antarctic Intermediate Water. Salt finger fluxes are estimated to be very large in

this region and similar to those documented in the Mediterranean outflow. Figs. 10 and 11 show the location of the BMC and CTD profiles of the region.

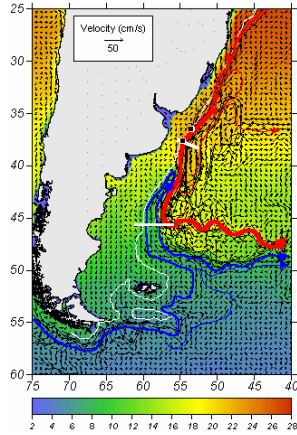


Figure 10. BMC including red (blue) line that is warm (cold) South Atlantic Central Water (Antarctic Intermediate Water)

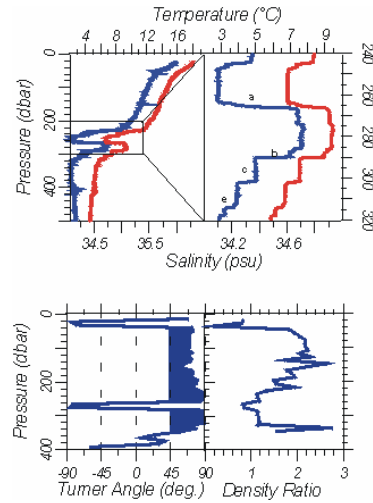


Figure 11. CTD observations from high spatial resolution surveys. Thermohaline staircases indicated by a,b,c, and e . Shaded region  $45 < Tu < 90$  correlates with  $1 < R_p < 2$  and indicates salt finger regime.

### c. East China Sea

A Chinese GLOBEC cruise in September 2003 took CTD profiles including vertical stratification of Kuroshio water. This particularly deep location of the study was situated on the continental slope. Water properties in Figure 12 indicate that above 140m the region is stable, and from 140-450m the depth dominate process is salt

fingers (where salinity and temperature both decrease with depth and turner angle between 45-90degrees). The region below 450m is also stable. The Kuroshio Current plays a role in stratifying this layer of water.

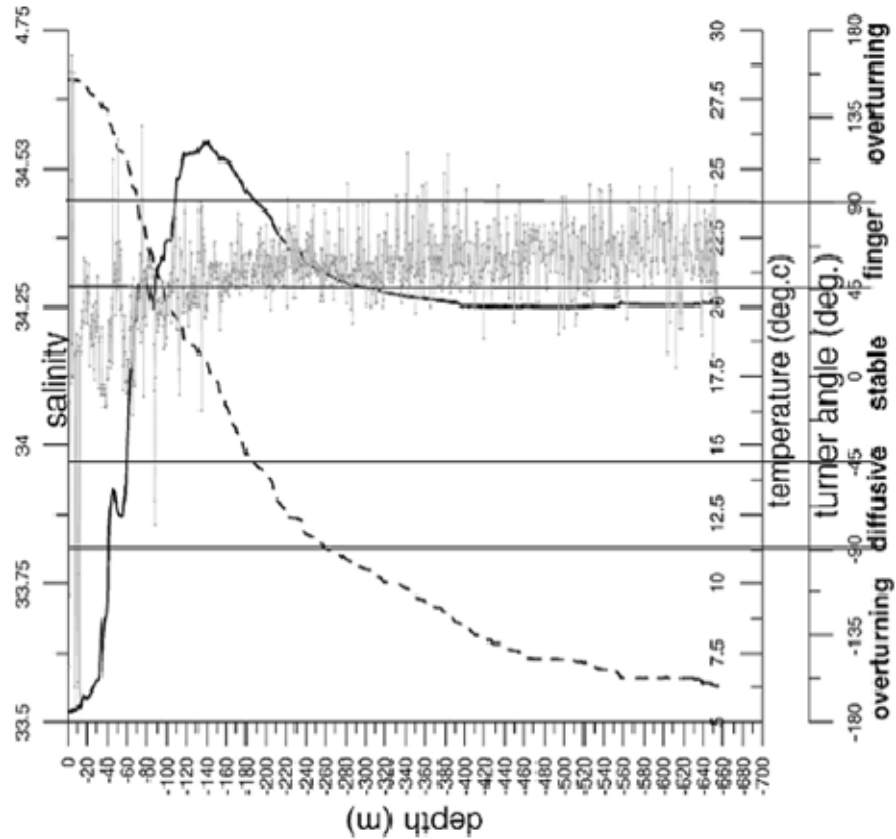


Figure 12. Vertical profiles of salinity (real line), temperature (dashed line), Turner angle (gray line) in the East China Sea at approximately 32N 129E (Shi and Wei, 2007).

### C. MEASURING MICROSTRUCTURE IN THE OCEAN.

The two quantities that have been commonly used in small-scale oceanography to characterize the intensity of diapycnal mixing are the dissipation rate of thermal variance ( $\chi_T$ ) and kinetic energy ( $\varepsilon$ ):

$$\chi_T = 2\kappa_T \left\langle \left( \frac{\partial T'}{\partial x} \right)^2 + \left( \frac{\partial T'}{\partial y} \right)^2 + \left( \frac{\partial T'}{\partial z} \right)^2 \right\rangle \quad (4)$$

$$\varepsilon = \frac{\nu}{2} \left\langle \left( \frac{\partial u_i}{\partial x_j} + \frac{\partial u_j}{\partial x_i} \right) \left( \frac{\partial u_i}{\partial x_j} + \frac{\partial u_j}{\partial x_i} \right) \right\rangle_{i,j=1 \text{ to } 3} \quad (5)$$

where  $u_i$  ( $i=1,2,3$ ) are the velocity components in x, y, and z directions,  $T'$  represents the micro-scale fluctuations in the vertical temperature,  $\kappa_T$  is the thermal diffusivity, and  $\nu$  is the molecular viscosity (Eqs 5). The dissipation of energy equation represents the rate of loss of KE of turbulent motion per unit mass through viscosity to heat. An obvious limitation for the direct application of Eqs. (4) and (5) to the analysis of the field data is related to the required knowledge of variation in  $T'$  and  $u_i$  in all spatial dimensions. Although such information is rarely available, attempts are commonly made to infer the dissipation rates by assuming that the statistics of variability in all dimensions are comparable. The errors associated with this assumption are discussed below.

#### D. ISOTROPIC ASSUMPTION

Unfortunately, the oceanographic probes only measure data vertically or horizontally which makes it impossible to compute the dissipation rates directly. The current method of quantifying the dissipation rates of thermal variance and kinetic energy is based on the isotropic assumption. If the variability of temperature or velocity is equivalent in all three directions; x, y, and z, then the dissipation rates of thermal and kinetic energy can be approximated as follows:

$$\chi_T = 2\kappa_T \left\langle \left( \frac{\partial T'}{\partial x} \right)^2 + \left( \frac{\partial T'}{\partial y} \right)^2 + \left( \frac{\partial T'}{\partial z} \right)^2 \right\rangle \approx 6\kappa_T \left\langle \left( \frac{\partial T'}{\partial z} \right)^2 \right\rangle \approx 6\kappa_T \left\langle \left( \frac{\partial T'}{\partial x} \right)^2 \right\rangle \quad (6)$$

$$\varepsilon = \frac{\nu}{2} \left\langle \left( \frac{\partial u_i}{\partial x_j} + \frac{\partial u_j}{\partial x_i} \right) \left( \frac{\partial u_i}{\partial x_j} + \frac{\partial u_j}{\partial x_i} \right) \right\rangle \approx \frac{15}{2} \nu \left\langle \left( \frac{\partial u}{\partial z} \right)^2 \right\rangle \approx \frac{15}{2} \nu \left\langle \left( \frac{\partial w}{\partial x} \right)^2 \right\rangle \quad (7)$$

Note that by using this assumption, horizontal temperature gradients are approximately equal to vertical temperature gradients. The proposed approximation resolves the immediate problem with quantifying the rates of dissipation from one-dimensional measurements, but a different concern arises with regard to its accuracy. Kantha and Clayson (2000) suggest that temperature fluctuations tend to be isotropic and homogeneous where turbulence is highly energetic and well developed, but not in general. With the collapse of turbulent motion in a stratified fluid, the energy containing eddies become strongly affected by buoyancy and fossilization results. Fossil turbulence is defined by Gibson (1988) as the remains of any fluctuation of temperature or salinity after (the inertial forces of) turbulent eddies are no longer dominant. When density changes are dominated by temperature variation, as is the case for salt fingers, they came to the conclusion that the isotropic assumption may lead to underestimates of the dissipation rates of thermal and velocity fluctuations ( $\varepsilon$  and  $\chi_T$ ) by factors of 2-4 (Thorpe, 2005).

While this isotropic assumption may be adequate for small-scale turbulence, it is possible that this reasoning is faulty in the realm of salt fingers. Most theoretical models suggest anisotropic, vertically elongated salt fingers (Stern, 1975; Schmitt; 1979a; Kunze, 1987). If salt fingers are indeed anisotropic, the equations (6) and (7) need to be corrected for the associated error. Once acknowledged, the question arises, at what value of  $R_\rho$  does the isotropic assumption cease to be valid?

In the lab, Taylor (1993) discovered that for  $R_\rho$  approaching 1, salt fingers tend to be more isotropic when growth rates are higher. This agrees with the numerical

experiments of Shen (1989) where at low  $R_\rho$  salt fingers are shorter, less organized, and have significant fluxes. Taylor also studied  $1 < R_\rho < 5$ , which showed that the average width to length ratio was 0.58, meaning his salt fingers were almost twice as long as they were wide. With this result, he suggests that the average vertical contribution to the temperature-gradient variance should be 0.34. This study seeks to understand when, why, and where it is acceptable to use this assumption and how best to correct for the error introduced.

## E. PROPOSED APPROACH

In order to correct for the error introduced by the isotropic assumption, the difference between the actual and approximated dissipation will be quantified by the anisotropic coefficients. We introduce four coefficients, two for each dissipation equation, which are denoted as  $A_{TV}$ ,  $A_{TH}$ ,  $A_{VV}$ ,  $A_{VH}$ , respectively.

$$\chi_T = 2\kappa_T \left\langle \left( \frac{\partial T'}{\partial x} \right)^2 + \left( \frac{\partial T'}{\partial y} \right)^2 + \left( \frac{\partial T'}{\partial z} \right)^2 \right\rangle \approx A_{TV} \cdot 6\kappa_T \left\langle \left( \frac{\partial T'}{\partial z} \right)^2 \right\rangle \approx A_{TH} \cdot 6\kappa_T \left\langle \left( \frac{\partial T'}{\partial x} \right)^2 \right\rangle \quad (8)$$

$$\varepsilon = \frac{\nu}{2} \left\langle \left( \frac{\partial u_i}{\partial x_j} + \frac{\partial u_j}{\partial x_i} \right) \left( \frac{\partial u_i}{\partial x_j} + \frac{\partial u_j}{\partial x_i} \right) \right\rangle \approx A_{VV} \frac{15}{2} \nu \left\langle \left( \frac{\partial u}{\partial z} \right)^2 \right\rangle \approx A_{VH} \frac{15}{2} \nu \left\langle \left( \frac{\partial w}{\partial x} \right)^2 \right\rangle, \quad (9)$$

where,

$$A_{TV} = \frac{\left\langle \left( \frac{\partial T'}{\partial x} \right)^2 + \left( \frac{\partial T'}{\partial y} \right)^2 + \left( \frac{\partial T'}{\partial z} \right)^2 \right\rangle}{3 \left\langle \left( \frac{\partial T'}{\partial z} \right)^2 \right\rangle}; \quad A_{TH} = \frac{\left\langle \left( \frac{\partial T'}{\partial x} \right)^2 + \left( \frac{\partial T'}{\partial y} \right)^2 + \left( \frac{\partial T'}{\partial z} \right)^2 \right\rangle}{3 \left\langle \left( \frac{\partial T'}{\partial x} \right)^2 \right\rangle}. \quad (10)$$

The anisotropic coefficient is thereby defined as the ratio of actual and approximated dissipation. These equations are used to calculate  $A_{TV}$  and  $A_{TH}$ . Similar equations may be used to calculate the coefficients of dissipation of kinetic energy,  $A_{VV}$  and  $A_{VH}$ . The simplest and most obvious technique to evaluate the anisotropic coefficients is numerical modeling. A key strength of the numerical realizations over their field or laboratory counterparts is the opportunity they provide to diagnose the variability of temperature and velocity fields in all spatial dimensions.

THIS PAGE INTENTIONALLY LEFT BLANK

## II. THE MODEL DESCRIPTION

Direct Numerical Simulations (DNS) were performed at the Naval Postgraduate School on a high performance cluster named Anastasia. Anastasia consists of five computing nodes. With eight computer processors (CPUs) per node, in total, there are forty CPUs that have the ability to work in parallel. We have performed a series of two-dimensional and three-dimensional computations.

Numerical modeling in two dimensions was beneficial for a couple of reasons. It was easier to resolve salinity scales in two dimensions. The process did not require parallel processing, and therefore, a large ensemble of calculations was successfully completed. The numerical model is a fully de-aliased pseudo-spectral FORTRAN code with message passing interface for three-dimensions, and a scalar version is used for two-dimensions. Integration in time uses the fourth order Runge-Kutta scheme and periodicity in all dimensions.

The first study examines salt finger growth in two dimensions, horizontal ( $x$ ), and vertical ( $z$ ). Following Radko and Stern (1999), temperature and salinity fields are decomposed into the linear basic state ( $\bar{T}$ ,  $\bar{S}$ ) and perturbations ( $T$ ,  $S$ ) from it. Simulations were initialized using random small amplitude temperature and salinity distributions.

The Boussinesq equations of motion were non-dimensionalized using  $d = \left( \frac{\kappa_T v}{g \alpha \bar{T}_z} \right)^{\frac{1}{4}}$  as the spatial scale,  $\frac{\kappa_T}{d}$  as the velocity scale,  $\frac{d^2}{\kappa_T}$  as the time scale,  $\kappa_T$  is the molecular diffusivity of heat,  $v$  is the kinematic viscosity,  $g$  is the gravitational acceleration,  $\alpha$  is the coefficient of thermal expansion,  $\bar{T}_z$  is the temperature gradient, and  $\alpha T_z d$  is the scale for both temperature and salinity perturbations. The result is the following non-dimensional set of governing equations:

$$\begin{aligned}
\frac{1}{\text{Pr}} \frac{dv}{dt} &= -\nabla p + \nabla^2 v + (T - S)\kappa, \\
\nabla \cdot v &= 0, \\
\frac{dT}{dt} + w &= \nabla^2 T, \\
\frac{dS}{dt} + \frac{1}{R_\rho} w &= \tau \nabla^2 S,
\end{aligned} \tag{11}$$

where  $\text{Pr} = \frac{\nu}{\kappa_T}$  is the Prandtl number,  $\tau = \frac{\kappa_S}{\kappa_T}$  is the Lewis number, and  $R_\rho$  is the background density ratio. The typical domain size resolved in our simulation was 50x50cm, and the typical (dimensional) duration of the simulation was approximately four days.

The time-step used to solve partial differential equations, is known to be limited by the Courant-Friedrichs-Lowy condition (CFL). In order for the simulation to produce reliable results, the time step must be less than a certain value. The CFL condition for pure advection schemes (one dimension) is given by:

$$\frac{u \Delta t}{\Delta x} < C \tag{12}$$

For a two-dimensional case this becomes:

$$\frac{u_x * \Delta t}{\Delta x} + \frac{u_y * \Delta t}{\Delta y} < C \tag{13}$$

The terms of the Courant ( C ) number include  $u$  as the velocity,  $\Delta t$  as the time step, and  $\Delta x$  as the length interval. The C term depends on a particular equation to be solved. For the simulations of double-diffusive convection, CFL condition can be reduced to

$$\Delta t \leq \frac{\Delta x}{C_{\max}} \quad (14)$$

where  $C_{\max}$  is the phase speed of the fastest growing salt finger. The models used in this study were tested with various non-dimensional time steps to determine how to run the model most efficiently. In agreement with Radko and Stern (1999), we have found that with decreasing  $R_\rho$ , the velocity amplitude increases and, therefore,  $\Delta t$  must be reduced to maintain the numerical stability.

THIS PAGE INTENTIONALLY LEFT BLANK

### III. DIRECT NUMERICAL SIMULATIONS IN TWO DIMENSIONS

In the following numerical simulations,  $\tau$  is systematically varied from 0.1-to-0.03-to-0.01,  $R_\rho$  is varied from  $R_\rho=1.1$  to 2.1 and Prandtl number is kept constant ( $\text{Pr}=7$ ). In the ocean  $\tau$  is 0.01, and so this study will focus on that value of  $\tau$  because it most resembles nature. The numerical simulations were extended in time until equilibrium was reached and sustained. In each case, the simulations were initiated by the small amplitude random computer generated T-S distribution. The flow was resolved by a uniform mesh with  $(N_x \times N_z) = (1024 \times 1024)$  elements. The size of the computational domain was chosen to resolve ten fastest growing finger wavelengths. The analysis of the flow patterns is based on the data recorded after the equilibration.

#### A. DEPENDENCE ON THE DENSITY RATIO

In order to quantify double diffusive dependence on density ratio alone,  $R_\rho$  is systematically increased between 1.1, 1.3, 1.5, 1.7, 1.9, and 2.1, while  $\tau$  is held constant at 0.03. At lower  $R_\rho$ , salt fingers are shorter and more disorganized. As  $R_\rho$  increases, salt fingers become more elongated and therefore more anisotropic. This is consistent with the theory of fastest growing finger model, Kunze (2003).

The plots shown in Figures 13-18 are representative of results after 450,000 time steps (or about four days). The figures below display four quantities: heat (blue line) and salt fluxes (green line) are shown below on the left, all flux values are negative numbers which correspond to the downward transport of heat and salt. Distribution of salinity and temperature are shown on the right. Warm salty water is red and cold fresh water is blue.

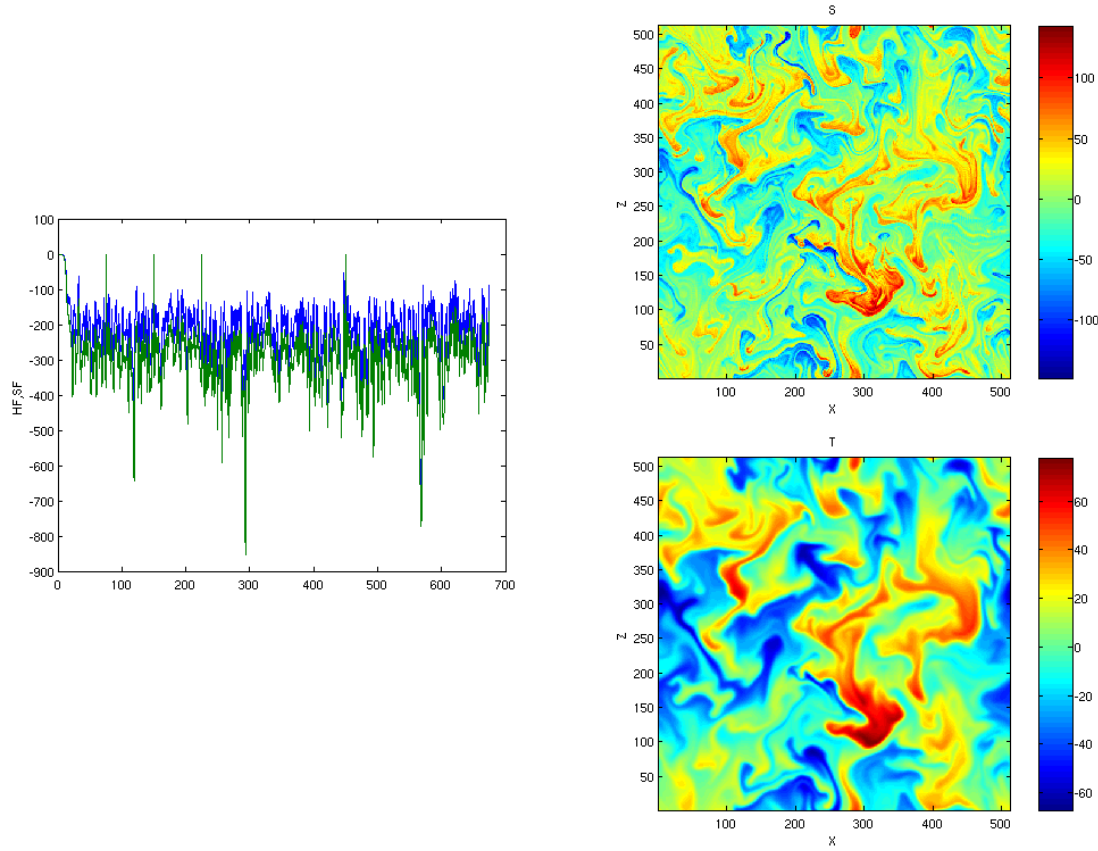


Figure 13. The non-dimensional heat and salt fluxes (left panel), distribution of salt (upper right) and temperature perturbation (lower right) for  $R_\rho = 1.1$ .

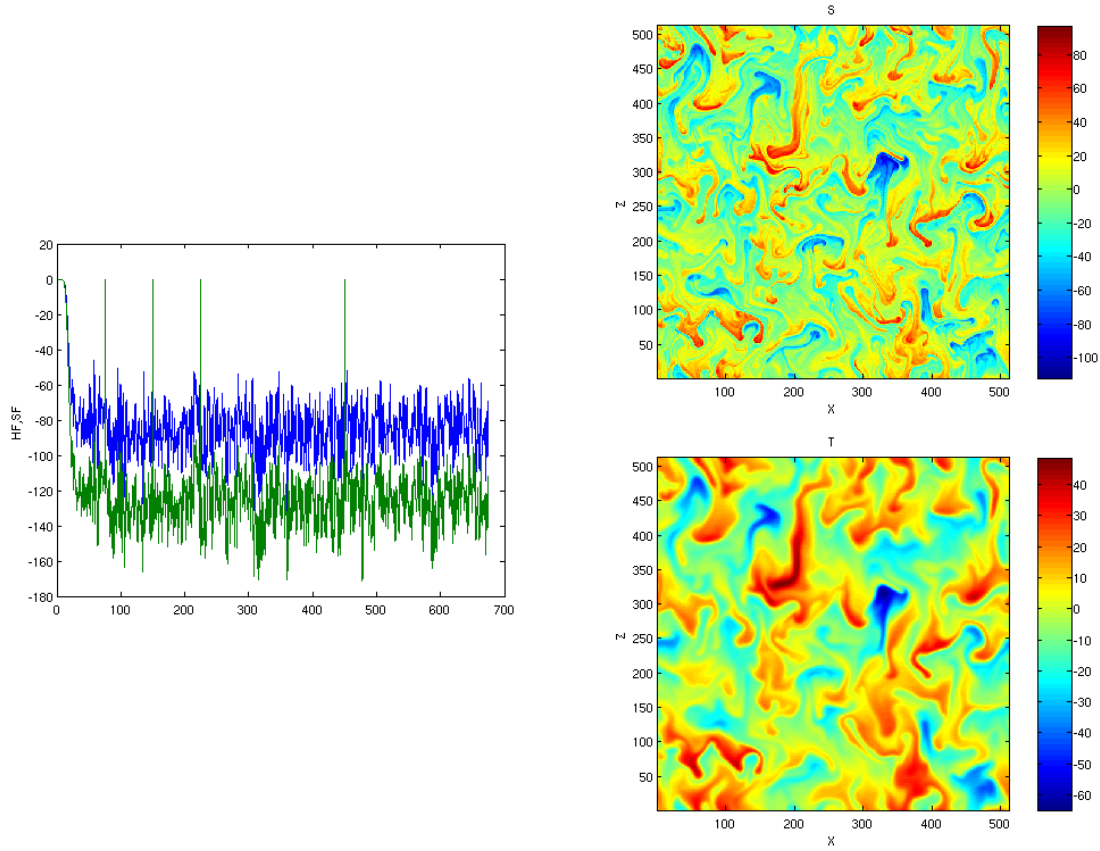


Figure 14. The same as in Fig.13 for  $R_\rho = 1.3$ .

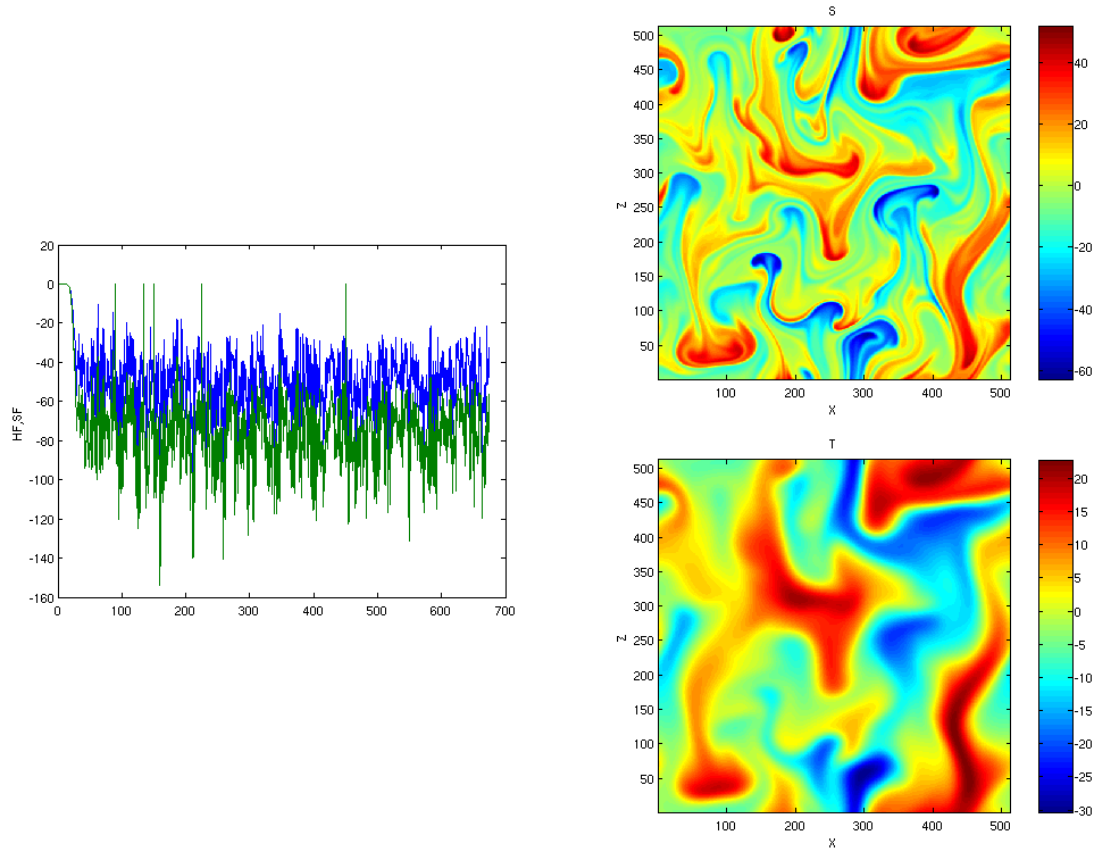


Figure 15. The same as in Fig.13 for  $R_\rho = 1.5$ .

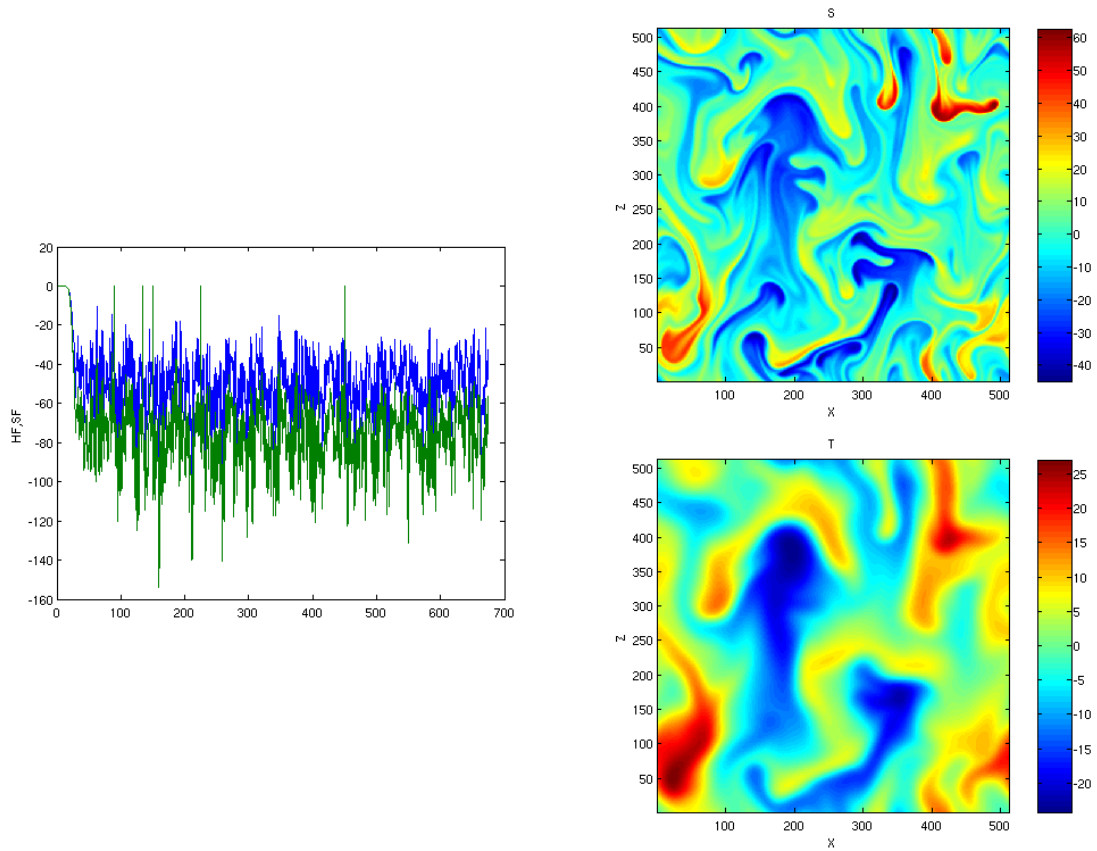


Figure 16. The same as in Fig.13 for  $R_\rho = 1.7$ .

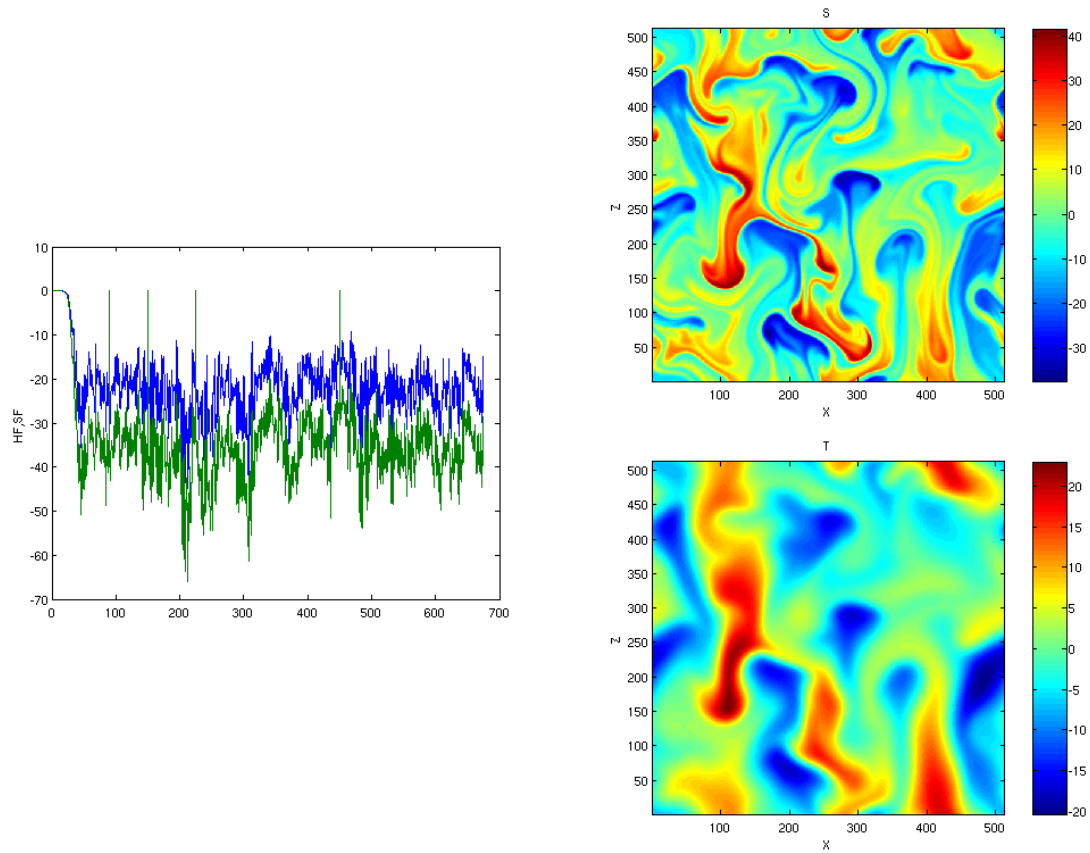


Figure 17. The same as in Fig.13 for  $R_\rho = 1.9$ .

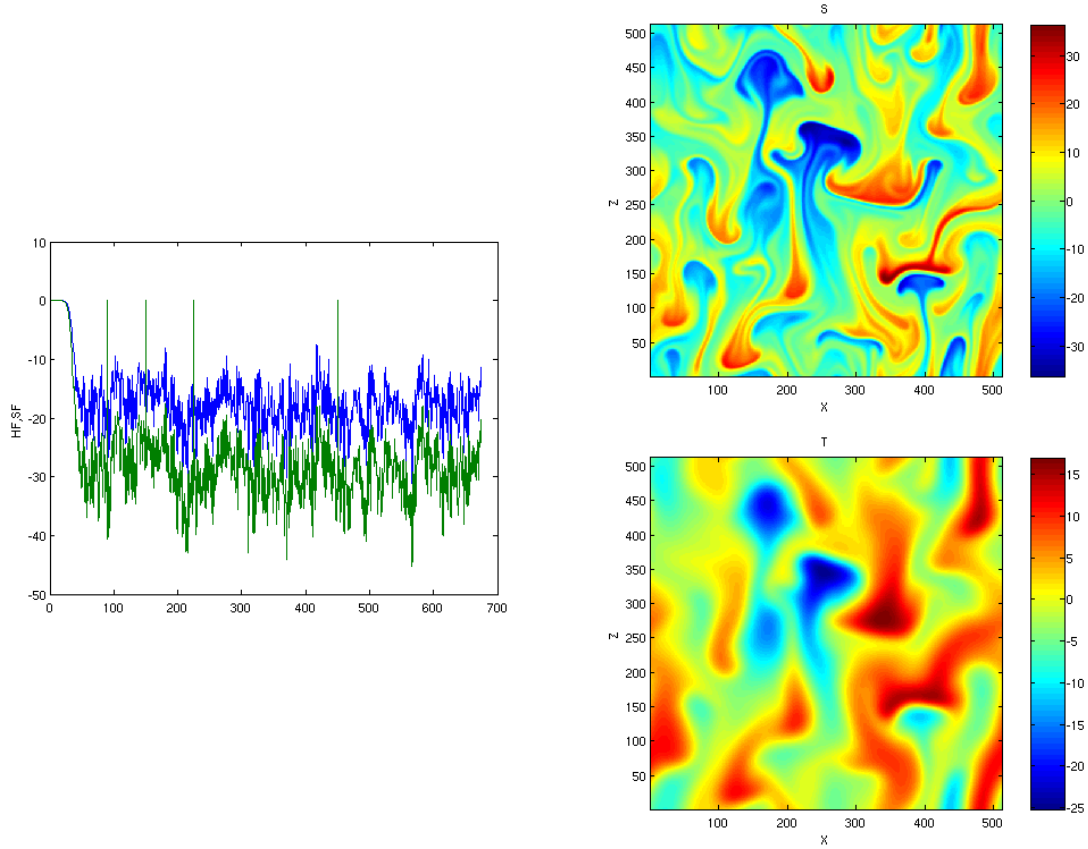


Figure 18. The same as in Fig.13 for  $R_\rho = 2.1$ .

## B. DEPENDENCE ON THE LEWIS NUMBER

The equilibrium state is achieved with the least amount of computational effort for  $\tau = 0.1$ ; however, this Lewis number is least realistic of an oceanic environment. It should be noted, however, that the increase in Lewis number is not expected to alter the fundamental physics and dynamics of salt fingering (Stern et. al., 2001), as long as  $\tau$  is considerably less than unity. For instance, many lab experiments have used a sugar-salt solution with  $\tau = 0.3$ , revealing the general similarity in the patterns of salt fingering with that for heat-salt value of  $\tau = 0.01$ .

In order to quantify if double diffusive convection has a dependence on diffusivity alone,  $\tau$  is systematically decreased between 0.1, 0.03, and 0.01, while density ratio is

held constant ( $R_\rho = 1.5$ ). The results shown in Figures 19-21 demonstrate that there are no fundamental differences of vertical fluxes, or temperature and salinity distributions seen below. Patterns appear to be fairly similar, regardless of the  $\tau$  used for each numerical simulation.

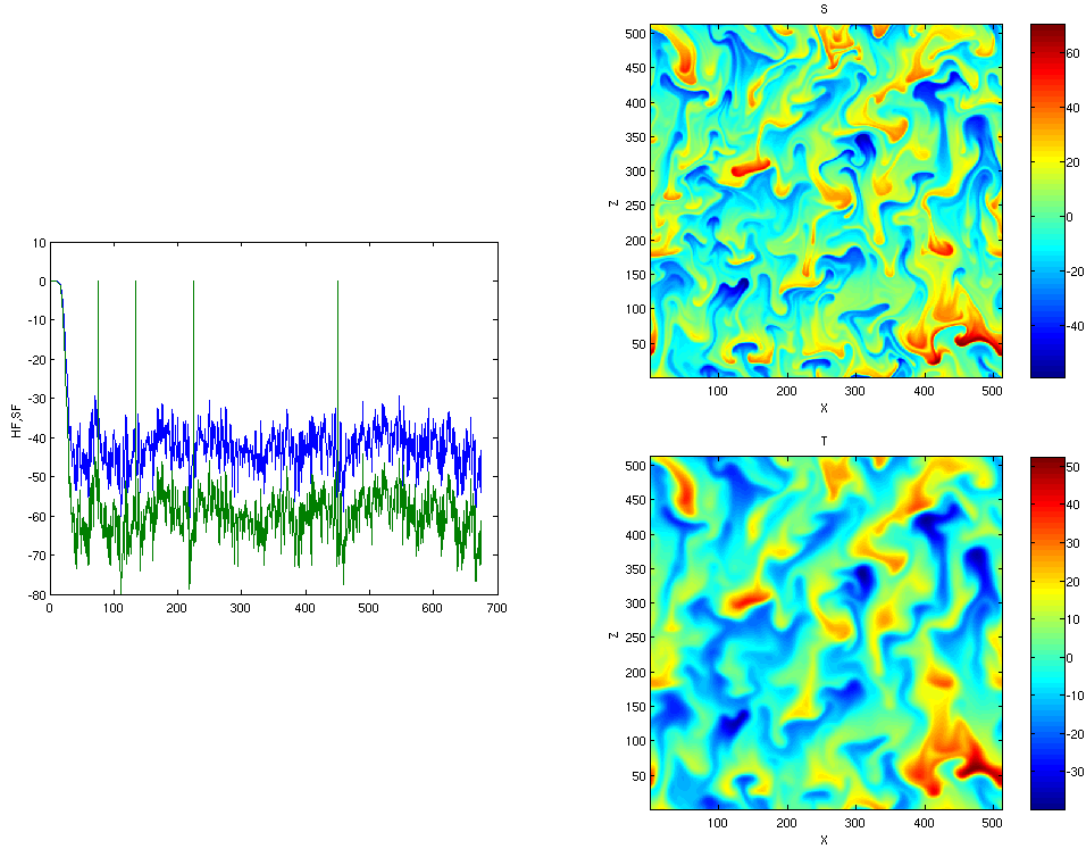


Figure 19. Same as Fig.13, however  $\tau=0.1$  and  $R_\rho=1.5$ .

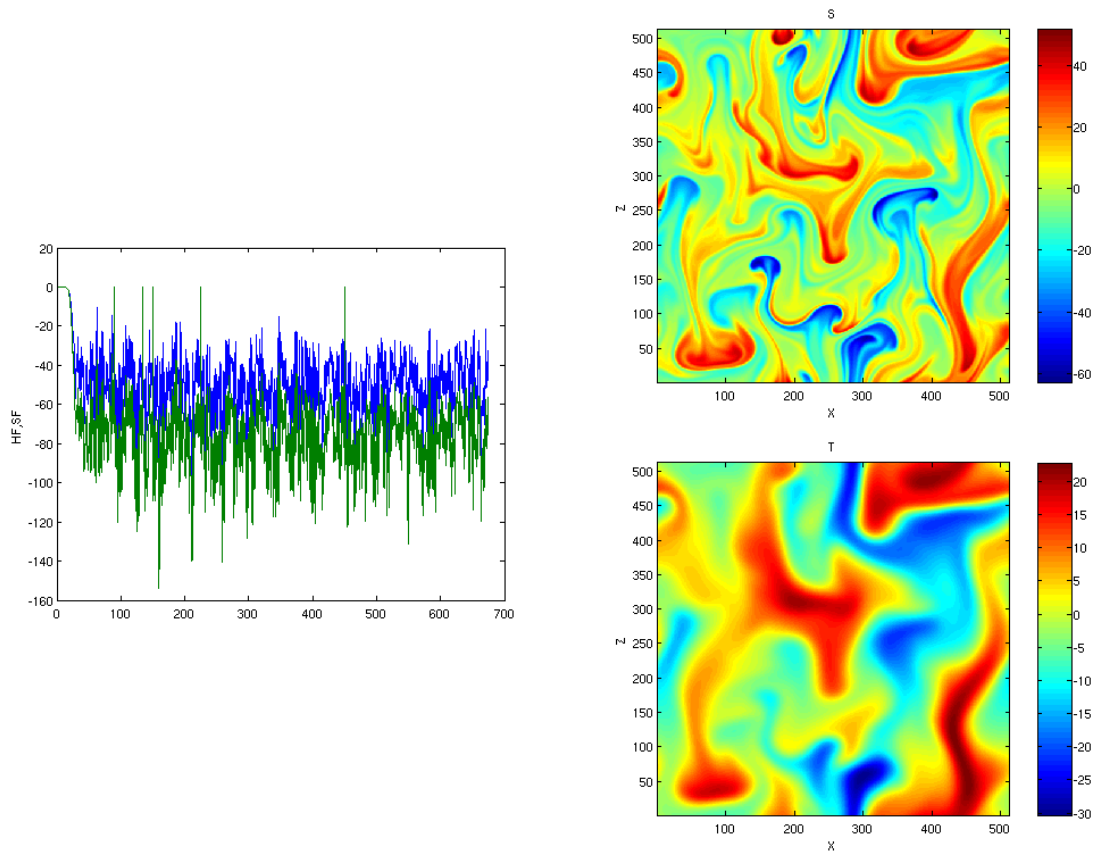


Figure 20. The same as in Fig.15.

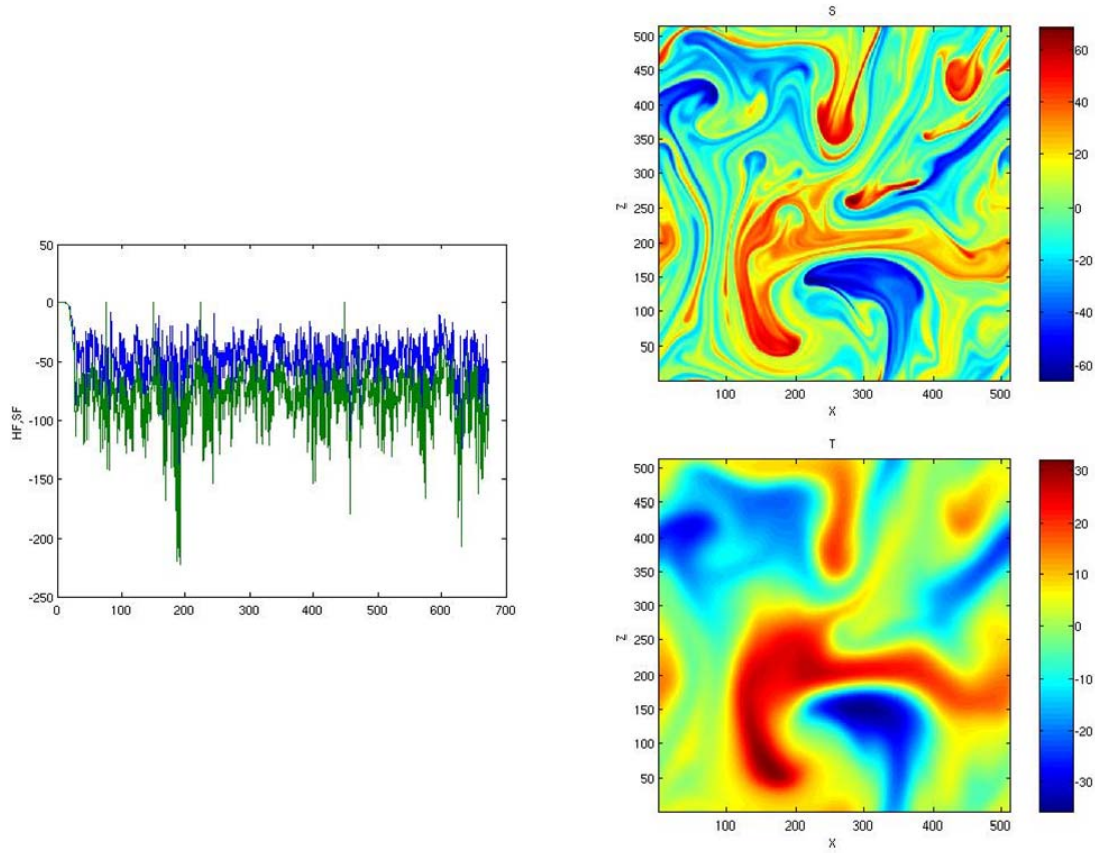


Figure 21. The same as in Fig.13, however  $\tau = 0.01$  and  $R_\rho = 1.5$ .

## IV. DIRECT NUMERICAL SIMULATIONS IN THREE DIMENSIONS

Modeling in three dimensions provides the most dynamic representation of nature. Although numerical capabilities dramatically increased over the past few decades, three dimensional simulations still pose a considerable computational challenge. The necessity of high performance parallel processing complicates modeling in three dimensions. By utilizing a third dimension, oceanographers may better understand salt-fingers; however, considerable difficulties arise with regard to resolving salinity dissipation scales.

Because of the two order difference in the molecular diffusivities of heat and salt ( $\tau \sim 0.01$ ) the salinity scale is considerably less by a factor of  $\frac{1}{\sqrt{\tau}} \sim 10$  than the characteristic finger width. The calculation with that resolution is currently not feasible given the existing computational resources. Therefore, all of the following calculations have been carried out using a larger value of  $\tau = 0.03$ .

### A. MODEL DESCRIPTION

For 3D simulations, we have used a fully de-aliased pseudo-spectral FORTRAN code with message passing interface originally developed by Oregon State University's ocean mixing group. The model has periodic boundary conditions in x, y, and z. Integration in time uses the fourth order Runge-Kutta scheme.  $\Delta t$  was adjusted for each experiment to ensure the CFL condition is met.

### B. DISTRIBUTION OF TEMPERATURE AND VERTICAL VELOCITY

As the plots of temperature (top) and vertical velocity (bottom) are most consistent they will be shown here. For simplicity, images shown below will include the xy (left) and xz (right) planes. Due to large computational requirements, only four model runs have been made. They are shown below. All boxes are 50cm by 50cm, red is warm and salty, blue is cold and fresh.

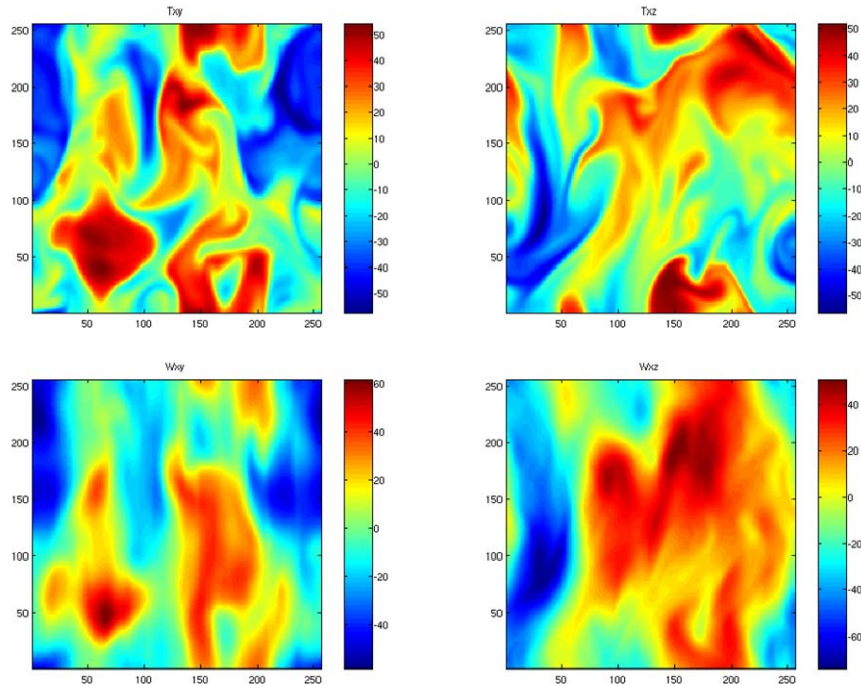


Figure 22. Temperature (top) and vertical velocity ('W' on bottom) in x-y (left) and x-z (right) planes, for  $R_\rho=1.1$ .

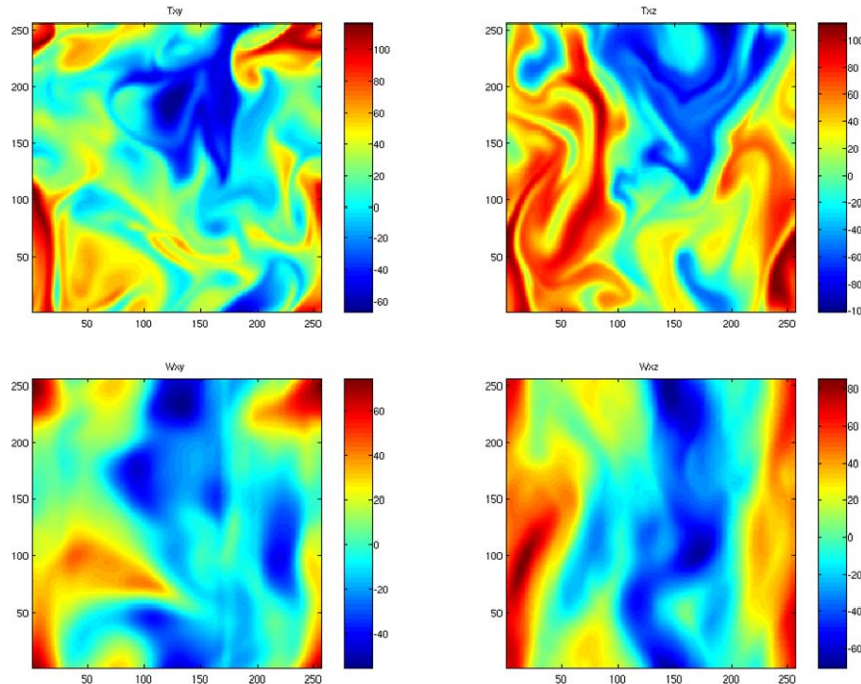


Figure 23. Same as Figure 22 above, for  $R_\rho = 1.3$ .

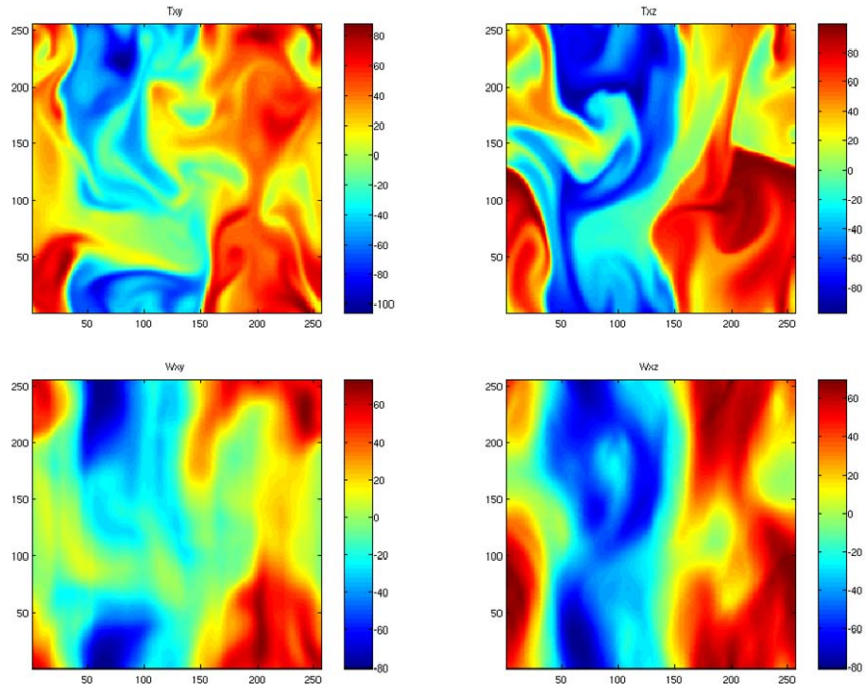


Figure 24. Same as Figure 22 above, for  $R_\rho = 1.5$ .

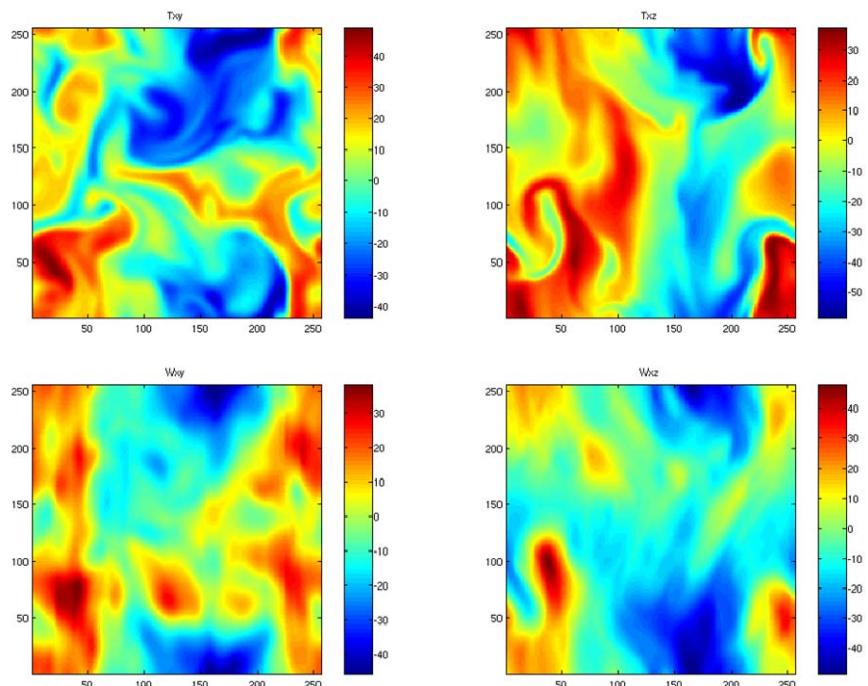


Figure 25. Same as Figure 22 above, for  $R_\rho = 1.9$ .

### C. EQUILIBRATION OF THE SALT FINGER MAGNITUDE

As mentioned earlier, our major goal is to examine the salt finger patterns in a fully equilibrated regime. In agreement with Radko and Stern (1999), we observed the nearly exponential growth of the salt finger amplitude at the beginning of each experiment. This exponential growth was followed by the nonlinear equilibration regime, as apparent in Fig. 26. Thus, anisotropic coefficients were calculated only during the period fluxes were in equilibrium. The stars in Figure 26 are located at a position of equilibrium which was defined by the second crossing of the temperature amplitude and its average equilibrated value.

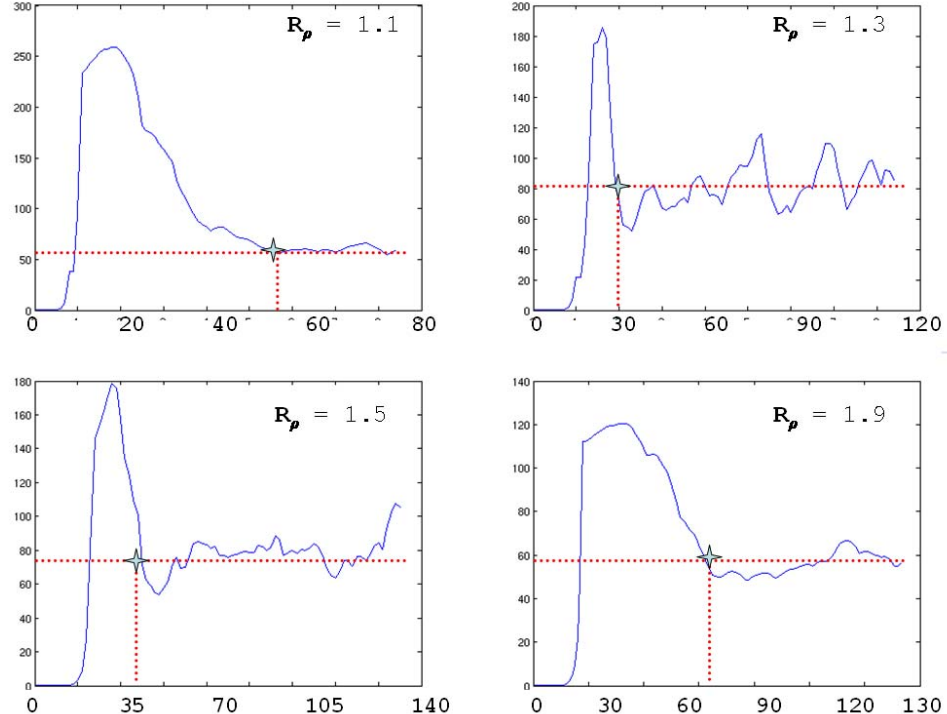


Figure 26. Maximum departure of temperature from the mean (non-dimensional value). Coefficients  $A_{TV}$ ,  $A_{TH}$ ,  $A_{VV}$ ,  $A_{VH}$  are calculated starting from the star, and on through equilibrium.

## V. RESULTS

Since our major goal is to quantify the statistically steady characteristics of double-diffusive convection for each experiment described in Sections III and IV, our analysis focused on the numerical data recorded after the equilibration of the initial growth of the temperature and salinity perturbations. In the following, we examine the dependencies of fluxes and the anisotropic coefficients on  $R_\rho$  and (for 2D calculations) on the Lewis number  $\tau$ .

### A. TWO DIMENSIONS

#### 1. Heat and Salt Fluxes

The heat and salt fluxes inferred from the 2D calculations are shown in Figs 27-30; black (white) columns indicate the values of the averaged heat (salt) flux. For each  $\tau$ , both heat and salt fluxes decrease with increasing  $R_\rho$ , which is consistent with the intuitive expectations that the activity of salt fingering increases dramatically as the stratification approaches the point of neutral static stability. The ratio of heat and salt fluxes are in agreement with the prediction of the fastest growing finger model (Schmitt, 1979b).

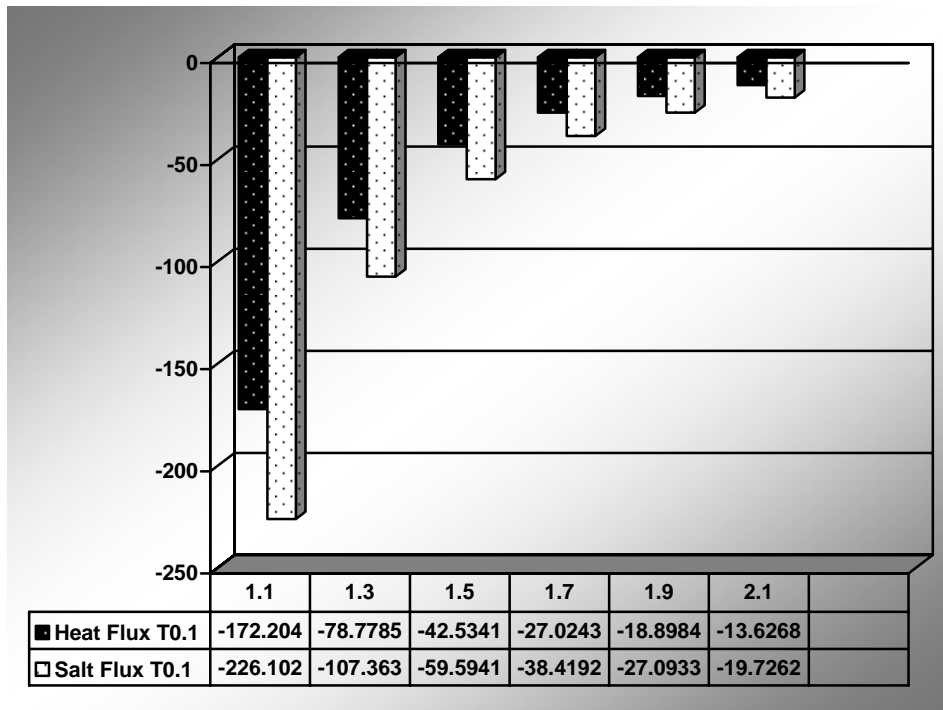


Figure 27. The non-dimensional heat and salt fluxes as a function of density ratio for  $\tau = 0.1$ . Note that both heat and salt fluxes decrease with  $R_p$ .

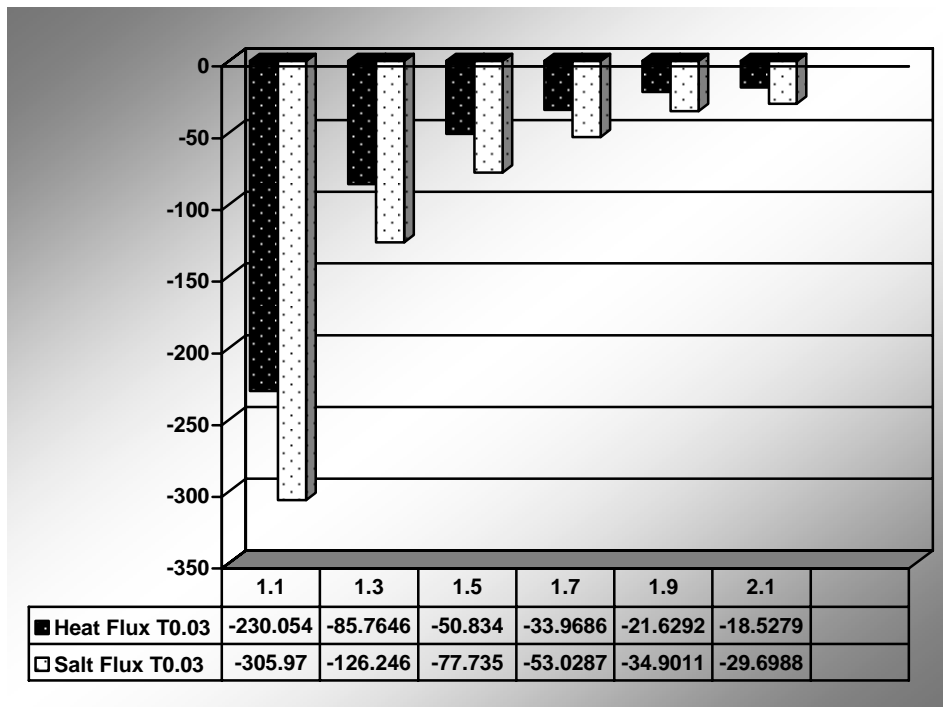


Figure 28. The same as in Fig. 27 but for  $\tau = 0.03$

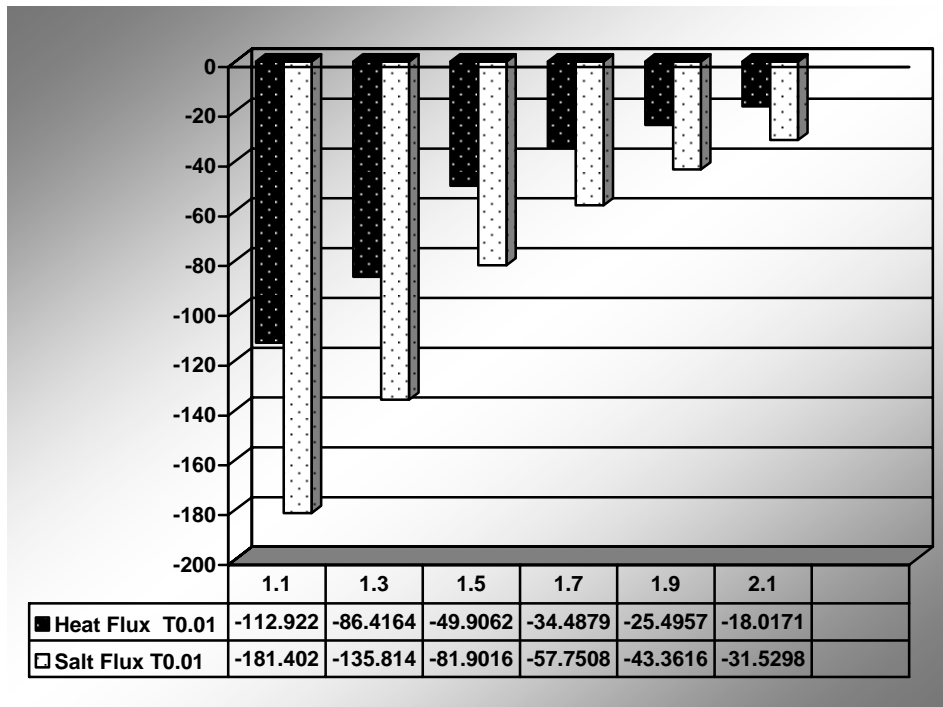


Figure 29. The same as in Fig. 27 but for  $\tau = 0.01$ .

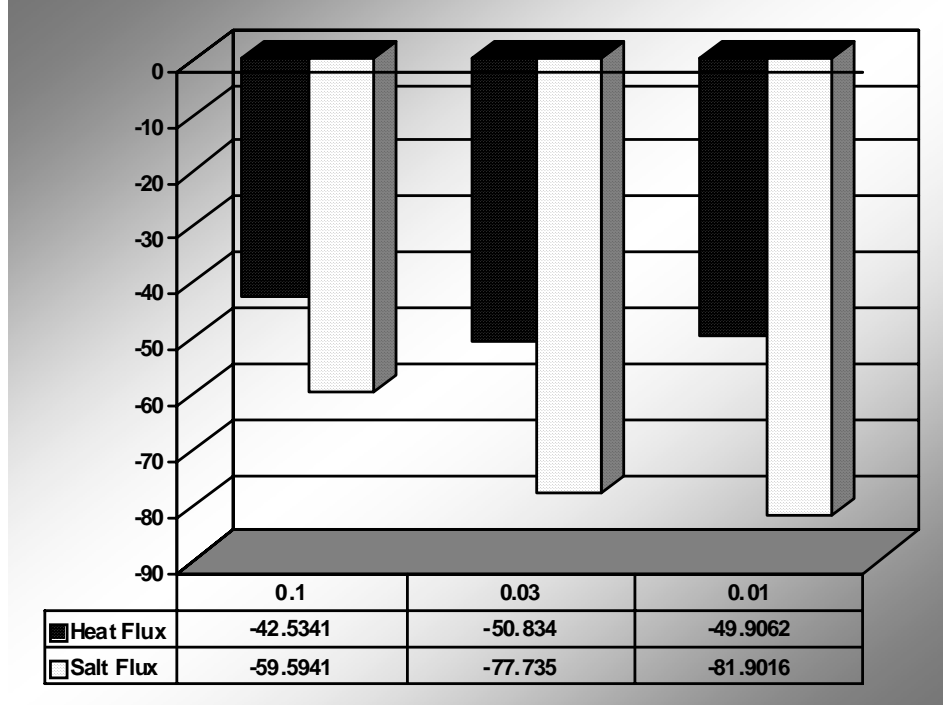


Figure 30. The non-dimensional heat and salt fluxes as a function of  $\tau$  for  $R_\rho = 1.5$ . Note the increase in fluxes with decreasing  $\tau$ .

## 2. Vertical Anisotropy of Salinity and Temperature

The vertical anisotropy coefficients of temperature and salinity are shown in Figs. 31-34. White (black) columns represent the vertical anisotropy of temperature (salinity). For each  $\tau$ , vertical anisotropy of temperature increases as density ratio increases. Note the difference between density ratio of 1.1 and 2.1. At density ratio 1.1, salt fingers are nearly isotropic and the vertical anisotropy coefficient is close to unity. However, as the density ratio increases to 2.1, the anisotropic coefficient for temperature grows to  $A_{TV}=1.4$ . This implies that the analysis of the microstructure measurements which does not take into account anisotropy of salt fingers, can result in an error as high as 40%.

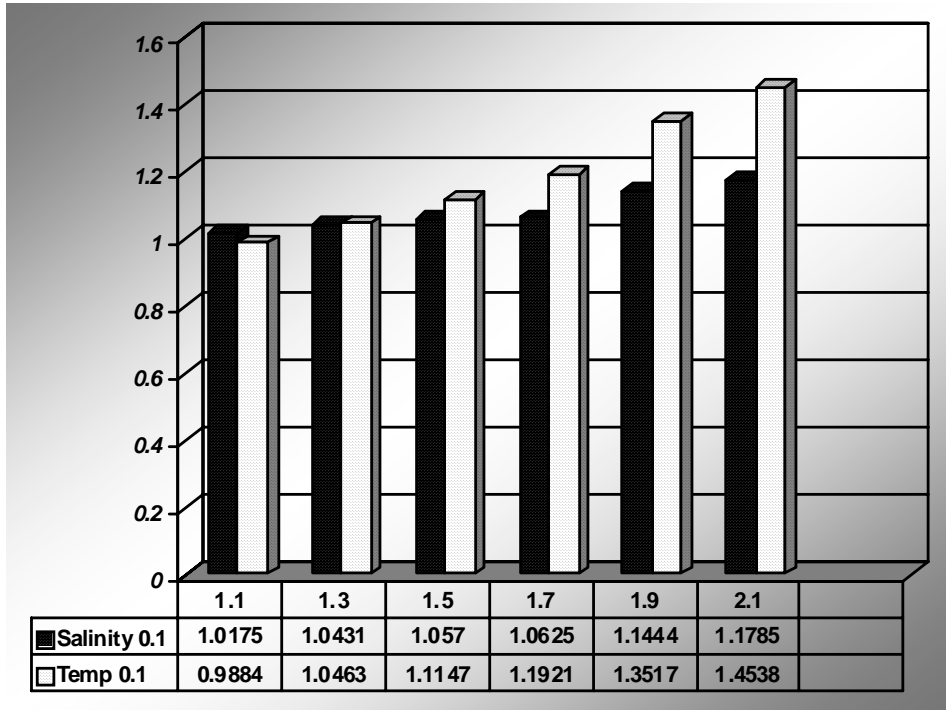


Figure 31. The vertical anisotropy coefficients for temperature ( $A_{TV}$ ) and salinity ( $A_{sv}$ ) as a function of the density ratio ( $R_\rho$ ) for  $\tau=0.1$ .

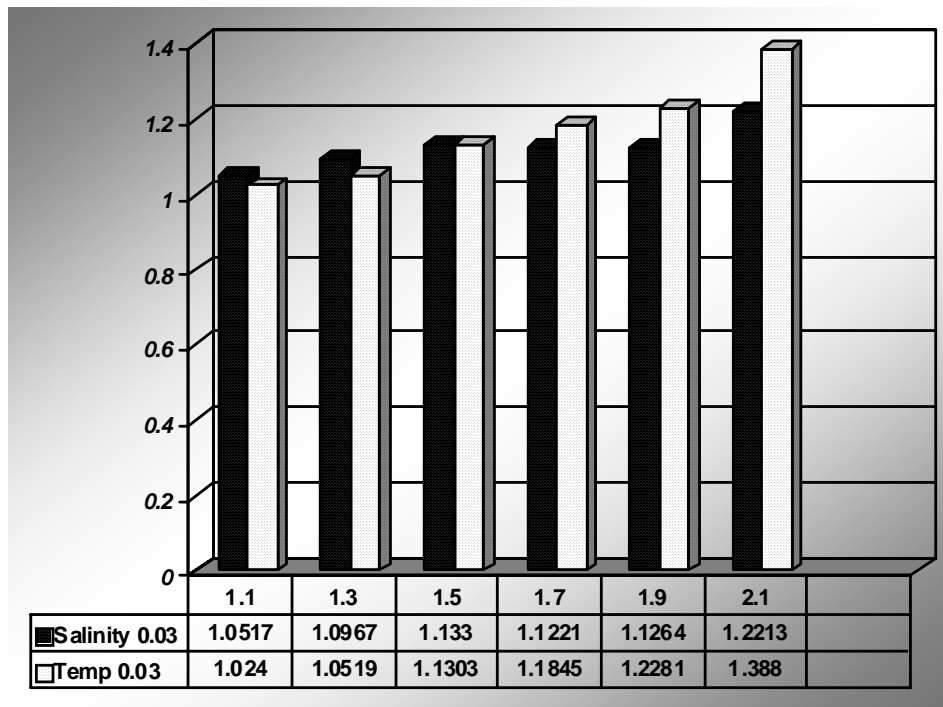


Figure 32. The same as in Fig. 31 but for  $\tau = 0.03$ .

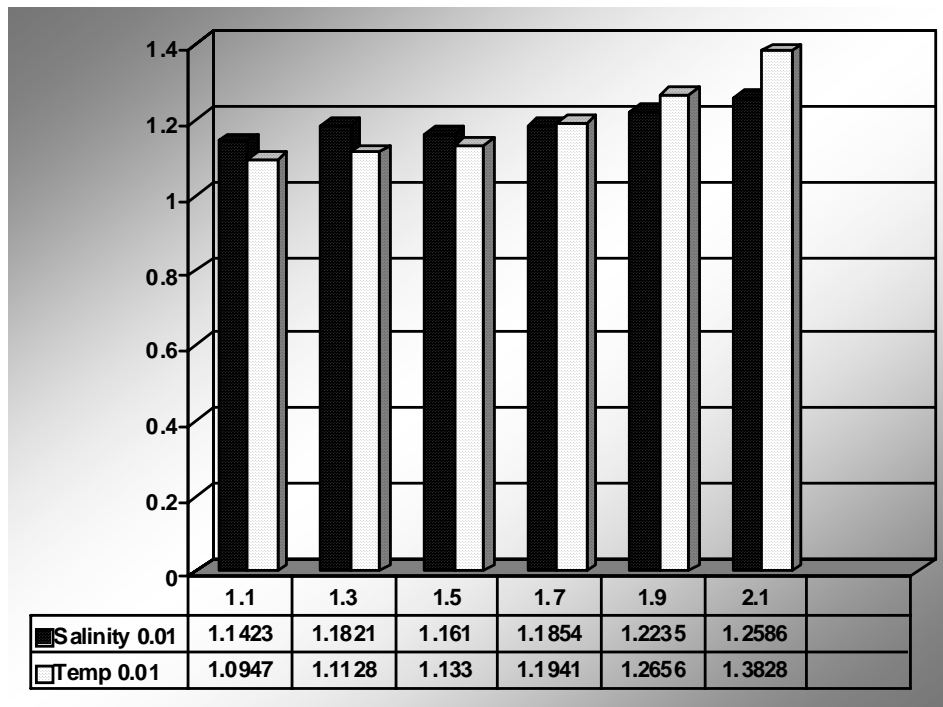


Figure 33. The same as in Fig. 31 but for  $\tau = 0.01$ .

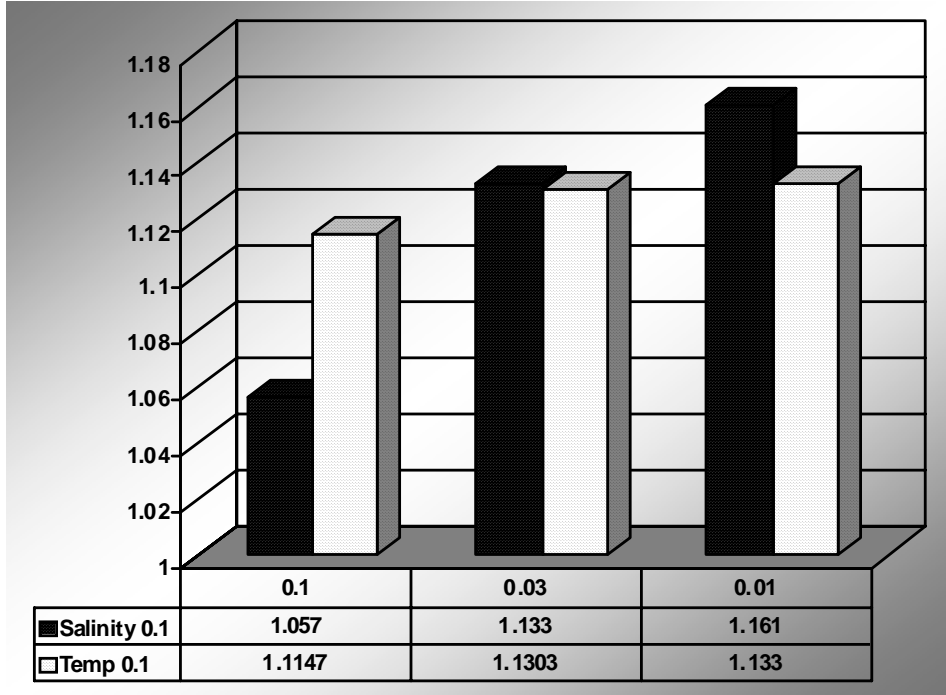


Figure 34. Vertical Anisotropy coefficients as a function of  $\tau$  for  $R_\rho=1.5$ .

### 3. Anisotropy of Velocity

In Figures 35-38, black (white) columns represent the anisotropy of velocity in the vertical (horizontal) direction. For each case, vertical anisotropy increases with  $R_\rho$  as horizontal anisotropy maintains or slightly decreases with  $R_\rho$ . Note that the anisotropy of velocity is by far more pronounced than the anisotropy of the temperature field.

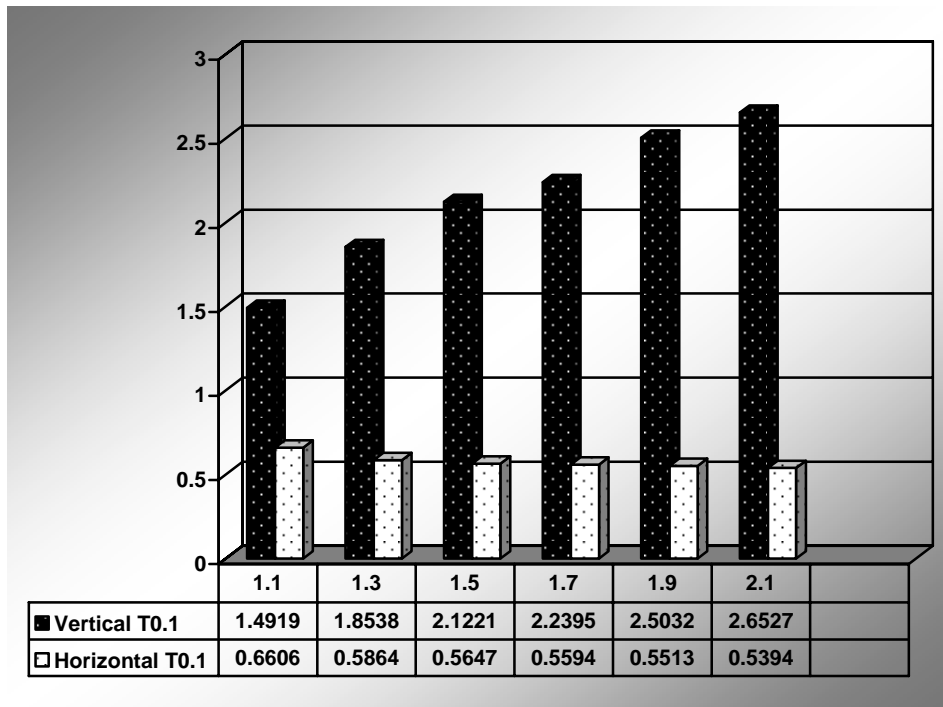


Figure 35. The anisotropy of velocity coefficients for vertical ( $A_{vv}$ ) and horizontal ( $A_{vh}$ ) directions, as a function of the density ratio ( $R_\rho$ ) for  $\tau = 0.1$ .

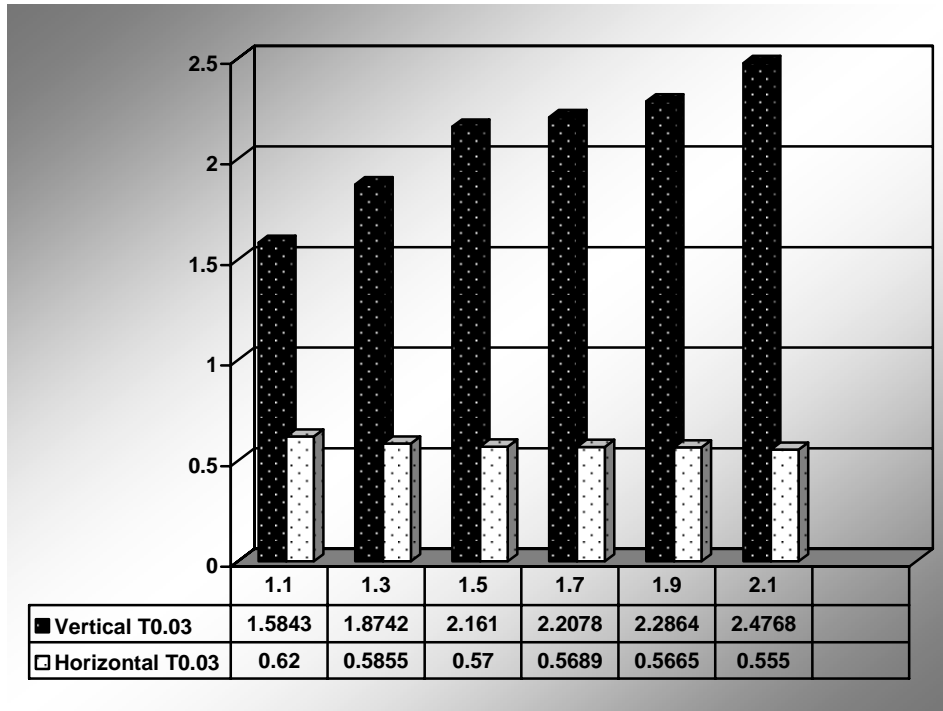


Figure 36. The same as in Fig. 35 but for  $\tau = 0.03$ .

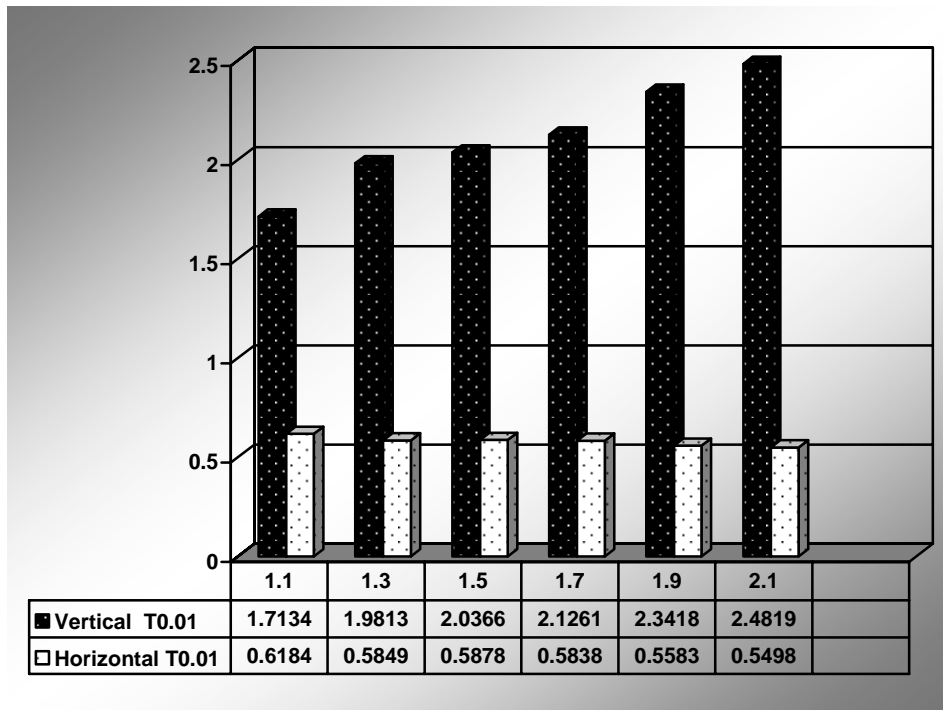


Figure 37. The same as in Fig. 35 but for  $\tau = 0.01$ .

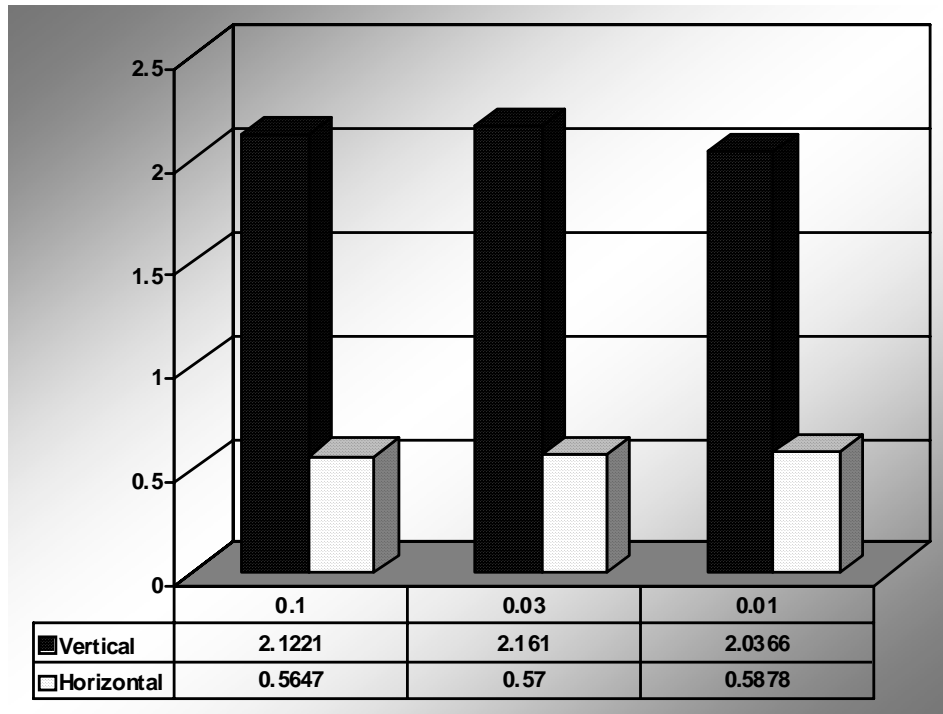


Figure 38. Anisotropy of velocity coefficients as a function of  $\tau$  for  $R_\rho = 1.5$ .

#### 4. Proposed Expressions for Temperature and Energy Dissipation

The foregoing analysis quantified the 2D anisotropy coefficients, which are summarized in Table 1.

Table 1. Proposed 2D anisotropic coefficients as a function of  $R_\rho$  for  $\tau = 0.01$

$R_\rho$	1.1	1.3	1.5	1.7	1.9	2.1
$A_{TV}$	1.0947	1.1128	1.133	1.1941	1.2656	1.3828
$A_{TH}$	0.9687	0.9559	0.9327	0.8871	0.8527	0.8183
$A_{VV}$	1.7134	1.9813	2.0366	2.1261	2.3418	2.4819
$A_{VH}$	0.6184	0.5849	0.5875	0.5838	0.5583	0.5498

This information leads to an attractive opportunity to evaluate the temperature and energy dissipation from one dimensional profiles using Eqs. (8), (9). It is assumed that the proposed anisotropy coefficients in Table 1 have a universal validity independent of the geographical location of measurements. Thus, for instance, for  $R_\rho = 2.1$ , Eqs. (8), (9), can be reduced (using Table 1) to

$$\chi_T \approx (1.4) \cdot 6\kappa_T \left\langle \left( \frac{\partial T}{\partial z} \right)^2 \right\rangle \approx (0.8) \cdot 6\kappa_T \left\langle \left( \frac{\partial T}{\partial x} \right)^2 \right\rangle \quad (15)$$

$$\varepsilon \approx (2.5) \frac{15}{2} \nu \left\langle \left( \frac{\partial u}{\partial z} \right)^2 \right\rangle \approx (0.5) \frac{15}{2} \nu \left\langle \left( \frac{\partial w}{\partial x} \right)^2 \right\rangle \quad (16)$$

Note that these expressions differ considerably from their isotropic counterparts Eqs. (6), (7) currently in use by the ocean mixing community. To insure that our conjectures are not biased by the two-dimensional nature of these simulations we consider a limited set of 3D experiments.

## B. THREE DIMENSIONS

### 1. Anisotropy of Salinity and Temperature

The vertical anisotropy coefficients of temperature and salinity are shown in Figures 39-41. White (black) columns represent the vertical anisotropy of salinity (temperature). Note the difference between density ratio of 1.1 and 2.1. At density ratio 1.1, salt fingers are isotopic when  $A_{TV}$  is equal to one. However, as density ratio increases to 1.9, the anisotropic coefficient grows to  $A_{TV}=1.2$ . This implies that conventional microstructure measurements which do not take anisotropy into account may yield approximately 20% error.

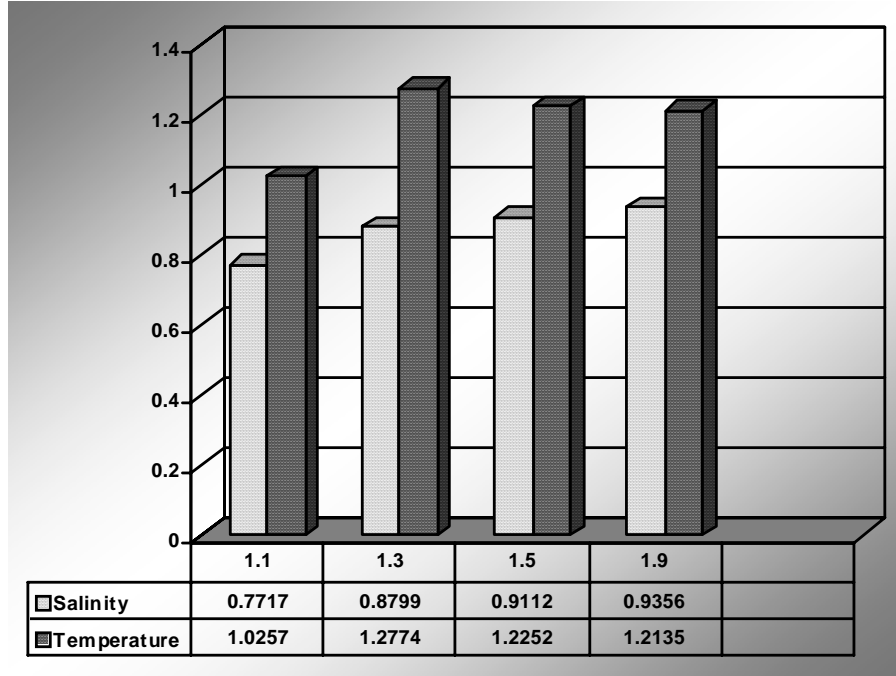


Figure 39. The 3D vertical anisotropy coefficients for temperature ( $A_{TV}$ ) and salinity ( $A_{SV}$ ) as a function of the density ratio ( $R_\rho$ ) for  $\tau=0.03$ .

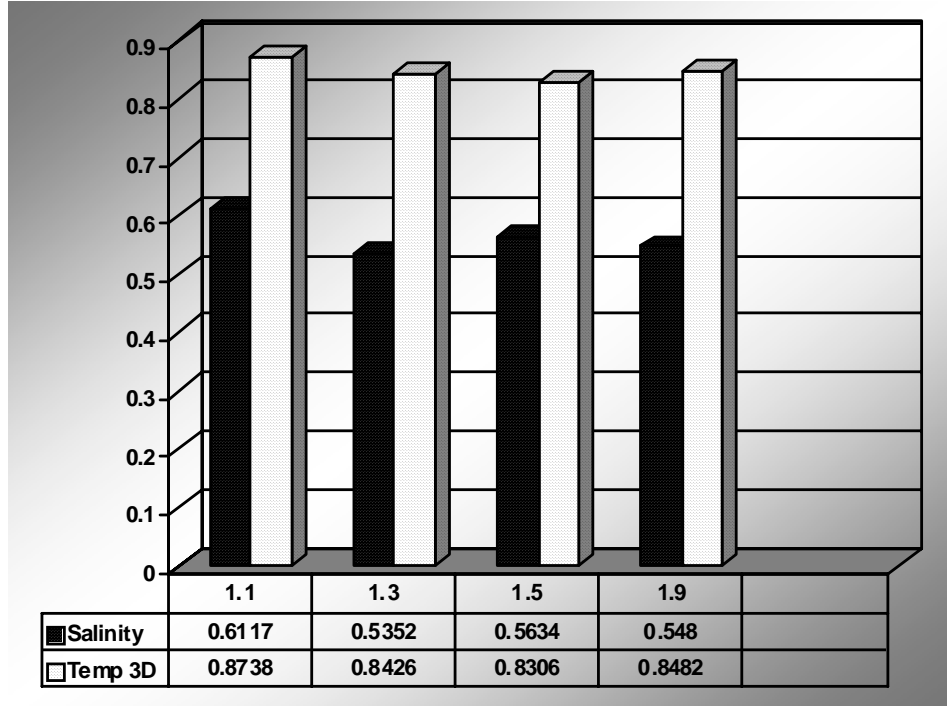


Figure 40. The horizontal anisotropy coefficients for temperature ( $A_{TH}$ ) and salinity ( $A_{SH}$ ) as a function of the density ratio ( $R_\rho$ ) for  $\tau = 0.03$ .

Black (white) columns in Fig. 41 are the anisotropy coefficients of velocity in the vertical (horizontal) direction. For each case, vertical anisotropy of velocity increases with  $R_\rho$  as horizontal anisotropy slightly decreases with  $R_\rho$ . Additionally, note that the anisotropy of velocity is much more pronounced than the anisotropy of the temperature field. These observations are consistent with the two dimensional numerical results.

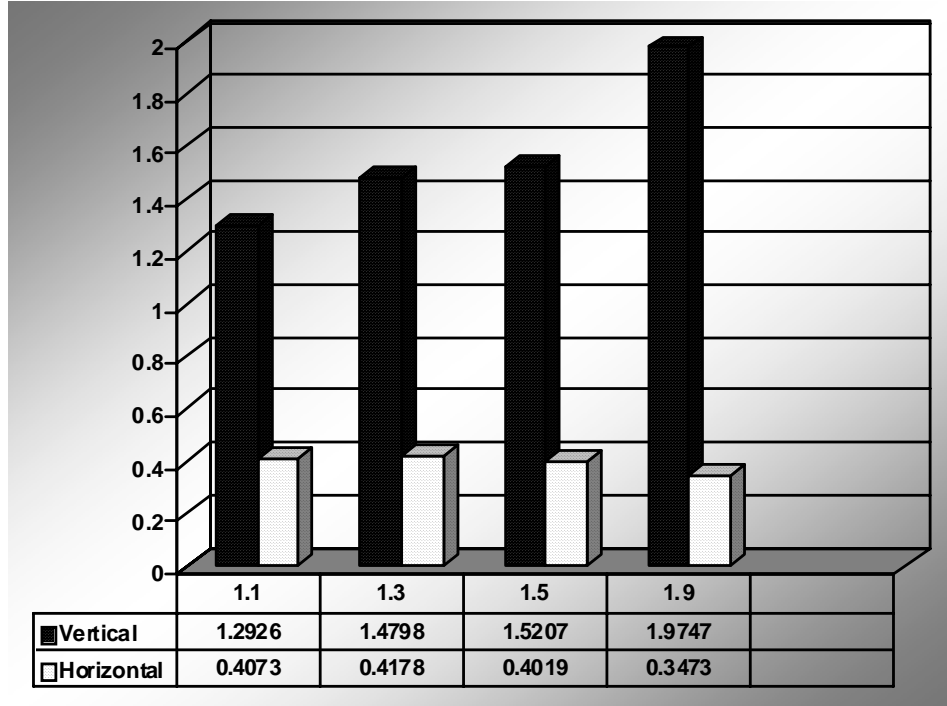


Figure 41. The anisotropy of velocity coefficients for vertical ( $A_{VV}$ ) and horizontal ( $A_{VH}$ ) directions as a function of density ratio for  $\tau = 0.03$ .

The 3D anisotropy coefficients are summarized in Table 1.

Table 2. Proposed 3D anisotropic coefficients as a function of  $R_\rho$  for  $\tau = 0.03$

$R_\rho$	1.1	1.3	1.5	1.9
$A_{TV}$	1.0257	1.2774	1.2252	1.2135
$A_{TH}$	0.8738	0.8426	0.8306	0.8482
$A_{VV}$	1.2926	1.4798	1.5207	1.9747
$A_{VH}$	0.4073	0.4178	0.4019	0.3473

It is assumed that the proposed anisotropy coefficients in Table 2 have a universal validity independent of the geographical location of measurements. Thus, for instance, for  $R_\rho = 1.9$ , Eqs (8),(9), can be reduced (using Table 2) to

$$\chi_T \approx (1.2) \cdot 6\kappa_T \left\langle \left( \frac{\partial T}{\partial z} \right)^2 \right\rangle \approx (0.8) \cdot 6\kappa_T \left\langle \left( \frac{\partial T}{\partial x} \right)^2 \right\rangle \quad (17)$$

$$\varepsilon \approx (2) \frac{15}{2} \nu \left\langle \left( \frac{\partial u}{\partial z} \right)^2 \right\rangle \approx (0.3) \frac{15}{2} \nu \left\langle \left( \frac{\partial w}{\partial x} \right)^2 \right\rangle \quad (18)$$

If anisotropic coefficients were not included in these equations as we've demonstrated, the conventional measurement of velocity dissipation would have 200% error. Similarly, if coefficient  $A_{TV}$  were omitted, then there would be about 20% error in conventional calculation of dissipation of temperature. Current isotropic assumptions do not account for these anisotropic coefficients, or the differences they represent in actual microstructure measurements.

### C. COMPARISON BETWEEN TWO AND THREE DIMENSIONAL SIMULATIONS

The inspection of Table 1 and Table 2 indicates that, in terms of the coefficients  $A_{TV}$ ,  $A_{TH}$ ,  $A_{VV}$ ,  $A_{VH}$ , the difference between two and three dimensional simulations is minor. This point is clear when comparing the recalibrated equations for  $\chi$  and  $\varepsilon$  in two and three dimensions for  $R_\rho = 1.9$  and  $\tau = 0.03$ :

$$\begin{aligned}\chi_T &\approx (1.23) \cdot 6\kappa_T \left\langle \left( \frac{\partial T'}{\partial z} \right)^2 \right\rangle \approx (0.86) \cdot 6\kappa_T \left\langle \left( \frac{\partial T'}{\partial x} \right)^2 \right\rangle \\ \varepsilon &\approx (0.55) \frac{15}{2} \nu \left\langle \left( \frac{\partial w}{\partial x} \right)^2 \right\rangle \approx (2.29) \frac{15}{2} \nu \left\langle \left( \frac{\partial u}{\partial z} \right)^2 \right\rangle\end{aligned}\tag{19}$$

$$\begin{aligned}\chi_T &\approx (1.21) \cdot 6\kappa_T \left\langle \left( \frac{\partial T'}{\partial z} \right)^2 \right\rangle \approx (0.84) \cdot 6\kappa_T \left\langle \left( \frac{\partial T'}{\partial x} \right)^2 \right\rangle \\ \varepsilon &\approx (0.35) \frac{15}{2} \nu \left\langle \left( \frac{\partial w}{\partial x} \right)^2 \right\rangle \approx (1.97) \frac{15}{2} \nu \left\langle \left( \frac{\partial u}{\partial z} \right)^2 \right\rangle\end{aligned}\tag{20}$$

The anisotropy coefficients differ by less than 10%, such a close agreement lends additional credence to both 2D and 3D calculations.

## VI. CONCLUSIONS

Vertical profilers used to record oceanic measurements are only capable of recording data vertically or horizontally. Because of this, oceanographers have had to generally analyze measurements of the microstructure, and similarly analyze double diffusion using the isotropic assumption. This assumption is motivated more by convenience rather than by the robust physical arguments. The isotropic assumption may be justified where turbulence is active and well developed but not in general, and particularly, not where the effects of stratification remain (Thorpe, 2005).

Our research has helped resolve some controversy regarding the use of the isotropy assumption in the analysis of the microstructure measurements, the magnitude of the heat and salt mixing rates, and their variation with environmental parameters.

The advent of high-resolution DNS made possible the ability to address the problem of salt finger anisotropy numerically. In particular, we performed a series of accurate two- and three-dimensional DNS of double diffusive convection in the parameter regime approaching that of the real ocean. We systematically decreased diffusivity ratio while varying background density ratio between  $R_\rho = 1.1$  and  $R_\rho = 2.1$ , and recorded its impact upon the anisotropic characteristics. Numerical results were then used to formulate a technique for reanalysis of the microstructure data. For the first time, a simple technique is proposed which takes anisotropy into account for both temperature and velocity fluctuations, and which is readily applicable to the field measurements. The proposed technique corrects the errors due to the isotropic assumption by providing the universal anisotropic coefficients ( $A_{TV}$ ,  $A_{TH}$ ,  $A_{VV}$ ,  $A_{VH}$ ). These coefficients describe temperature and velocity fluctuations vertically and horizontally. When density ratio was systematically increased, salt fingering became more regular and elongated, and vertical anisotropy coefficients increased. The proposed universal anisotropic coefficients are dependent upon  $R_\rho$ .

In agreement with the intuitive expectations preliminary calculations, it has been shown herein that anisotropy effects are significant and must be taken into account in microstructure measurements. Results from this experiment are consistent with the tendency of salt fingers to become more regular and elongated for large  $R_\rho$ , and more chaotic for low  $R_\rho$ . Results are not particularly sensitive to the diffusivity ratio or the number of spatial dimensions.

Failure to take anisotropy into account can result in errors in excess of 100% for dissipation of thermal variance, and errors in excess of 200% for dissipation of kinetic energy.

The ability to recognize the regions of active double-diffusive convection and to quantify its intensity is important in many naval applications. Of particular concern are (i) the acoustic remote sensing in the double-diffusive ‘staircase’ regions and (ii) the accurate representation of double-diffusive mixing in the large-scale models simulating the battle space environment. It has been shown that thermohaline staircases affect sound propagation whether the sound source originates from within (or outside) of the staircase region, especially at high frequency. With regard to the general oceanographic significance of this work, we note that small-scale mixing plays a fundamental role in the ocean’s ability to transport heat, nutrients, pollutants and carbon dioxide. Thus, advances in understanding double-diffusive transport will improve climate and ecosystem modeling capabilities that will have clear societal benefits.

## VII. FUTURE STUDIES

If this study is continued in the future there are a few recommendations. First, it is recommended to continue modeling in three dimensions. Before doing so, it is important to allocate a very large computing resource that won't put prohibitive limits on the number of experiments and the spatial resolution. There are resources available outside of the Naval Postgraduate School which would make it possible to fully resolve all the relevant scales in double diffusive convection.

Second, in future experiments, one should explore the parameter range in more detail. One example of that would be to include background shear. In the ocean, there exists background shear, and that has not been taken into account in our preliminary analysis.

Third, there should be further critical reanalysis of the existing microstructure measurements of double diffusive mixing. The proposed technique should be applied directly to the field data. Since the background density ratio is readily available from these measurements, it should be possible to recalculate the vertical heat/salt mixing rates and diffusivities using our empirical anisotropy coefficients for all measurements taken in the regions of active salt fingering. It would be most beneficial to map out areas of the world ocean where the anisotropy of salt fingers has to be taken into account.

Finally, a long-term goal is to create a physically based parameterization of double diffusion for large-scale ocean models. Doing this might better explain large scale effects salt fingers may have on global climate and circulation patterns.

THIS PAGE INTENTIONALLY LEFT BLANK

## LIST OF REFERENCES

Bianchi, A. A., Piola, A. R., and Collino, G. J. (2002). Evidence of double diffusion in the Brazil-Malvinas Confluence. *Deep-Sea Research I*, 49, 41-52.

Gibson, C. (1988). Evidence and consequences of fossil turbulence in the ocean. *Small-Scale Turbulence and Mixing in the Ocean*, ed. J.C.J. Nihoul and B.M. Jamart. Amsterdam: Elsevier, pp. 319-334.

Kantha, L. H., and Clayson, C. A. (2000). *Small Scale Processes in Geophysical Fluid Flows*. Academic Press, San Diego, CA, 888 pp.

Kluikov, Y. Y., and Karlin, L. N. (1995). A model of the ocean thermocline stepwise stratification caused by double diffusion. *Double Diffusive Convection-Geophysical Monograph*. 94. 287-303.

Kunze, E. (1987). Limits on growing, finite lengths salt fingers: A Richardson number Constraint. *J. Mar. Res.* 45. 533-556.

Kunze, E. (2003). A review of oceanic salt-fingering theory. *Progress in Oceanography*. 56. 399-417.

Piacsek, S. A., and Toomre, J. (1980). Nonlinear evolution and structure of salt fingers. In J. C. J. Nihoul (Ed.), *Marine turbulence* (193-219). *Elsevier oceanography series*, 28.

Prikasky, I. J. (2007). Direct Numerical Simulation of the Diffusive Convection and assessment of its impact on arctic climate change. Published Master of Science in Meteorology and Physical Oceanography Thesis, Naval Postgraduate School, Monterey, CA.

Radko, T., and Stern, M. E. (1999). Salt fingers in three dimensions. *J. Mar. Res.* 57. 471-502.

Ruddick, B. R. (1983). A practical indicator of the stability of the water column to double-diffusive activity. *Deep Sea Res.*, 30, 1105-1107.

Schmitt, R. W. (1979a). Flux measurements on salt fingers at an interface. *J. Mar. Res.* 37, 419-436.

Schmitt, R. W. (1979b). The growth rate of supercritical salt fingers. *Deep Sea Research*, 26A, 23-44.

Schmitt, R. W., Ledwell, J., Montgomery, E.T., Polzin, K., Toole, J. (2005). Enhanced diapycnal mixing by salt fingers in the main thermocline of the tropical Atlantic. *Science*, 306, 385-388.

Shen, C. Y. (1989). The evolution of the double-diffusive instability: salt fingers. *Physics of Fluids A*, 5, 829-844.

Shi, J. and Wei, H. (2007). Evidence of double diffusion in the East China Sea. *J. Mar. Sys.*, 67, 272-281.

Stern, M. E. (1960). The “salt fountain” and thermohaline convection. *Tellus*, 12, 172-175.

Stern, M. E. (1975). *Ocean Circulation Physics*. Academic Press, NY.

Stern, M. E., Radko, T., and Simeonov, J. (2001) Salt Fingers in an unbounded thermocline. *J. Mar. Res.*, 59, 335-390.

Stommel, H. M., Arons, A. B., Blanchard, D. (1956). An oceanographic curiosity: The perpetual salt fountain. *Deep-Sea Res.*, 3, 152-153.

Tait, R. I., and Howe, M. R. (1968). Some observations of thermohaline stratification in the deep ocean. *Deep Sea Research*, 15, 275-280.

Tait, R. I. and Howe, M. R. (1971). *Nature*, London, 231, 178-179.

Taylor, J. R. (1993). Anisotropy of Salt Fingers. *J. of Physical Oceanography*, 23, 554-565.

Thorpe, S. A. (2005). *The Turbulent Ocean*. Cambridge University Press, Cambridge, UK, 439 pp.

Turner, J. S. (1965). The coupled turbulent transports of salt and heat across a sharp density interface. *Int. J. Heat Mass Transfer*, 6, 759-767.

Turner, J. S. (1973). *Buoyancy Effects in Fluids*. Cambridge University Press, Cambridge, UK, 276

Turner, J. S., and H. Stommel. (1964). A new case of convection in the presence of combined vertical salinity and temperature gradients. *Proc. Natl. Acad. Sci.* 52, 49-53.

Wall, S.E. (2007). Structure and evolution of thermohaline staircases in tropical North Atlantic. Published Master of Science in Physical Oceanography Thesis, Naval Postgraduate School, Monterey, CA.

Williams, A. J. (1974). Salt Fingers observed in Mediterranean outflow. *Science*, 185, 941-943.

You, Y. (2002). A global ocean climatological atlas of the Turner angle: Implications for double-diffusion and water mass structure. *Deep-Sea Res.*, 49, 2075-2093.

Yoshida, J., and Nagahsima H. (2003). Numerical experiments on salt-finger convection. *Progress in Oceanography*, 56, 435-459.

Zhang, J., and Schmitt, R. W. (2000). The impact of salt fingering on the Thermohaline Circulation under mixed boundary conditions. *J. of Physical Oceanography*, 30, 1223-1231.

THIS PAGE INTENTIONALLY LEFT BLANK

## **INITIAL DISTRIBUTION LIST**

1. Defense Technical Information Center  
Ft. Belvoir, Virginia
2. Dudley Knox Library  
Naval Postgraduate School  
Monterey, California
3. Dr. Mary L. Batteen  
Naval Postgraduate School  
Monterey, California
4. Dr. Timour Radko  
Naval Postgraduate School  
Monterey, California
5. Dr. Jeff Haferman  
Naval Postgraduate School  
Monterey, California